

Modelling non-stationarity in asymptotically independent extremes

C. J. R. Murphy-Barltrop^{1*} and J. L. Wadsworth²

¹STOR-i Centre for Doctoral Training, Lancaster University LA1 4YR, United Kingdom

²Department of Mathematics and Statistics, Lancaster University LA1 4YF, United Kingdom

*Correspondence to: c.barltrop@lancaster.ac.uk

March 21, 2022

Abstract

In many practical applications, evaluating the joint impact of combinations of environmental variables is important for risk management and structural design analysis. When such variables are considered simultaneously, non-stationarity can exist within both the marginal distributions and dependence structure, resulting in complex data structures. In the context of extremes, few methods have been proposed for modelling trends in extremal dependence, even though capturing this feature is important for quantifying joint impact. Motivated by the increasing dependence of data from the UK Climate Projections, we propose a novel semi-parametric modelling framework for bivariate extremal dependence structures. This framework allows us to capture a wide variety of dependence trends for data exhibiting asymptotic independence. When applied to the climate projection dataset, our model is able to capture observed dependence trends and, in combination with models for marginal non-stationarity, can be used to produce estimates of bivariate risk measures at future time points.

Keywords: Extremal Dependence, Non-stationary Processes, Multivariate Extremes

1 Introduction

Modelling joint tail behaviour of multivariate datasets is important in a wide variety of applications, including nuclear regulation (Office for Nuclear Regulation, 2018), neuroscience (Guerrero et al., 2021) and flood risk analysis (Gouldby et al., 2017). When analysing multivariate extremes, it is important to capture the dependence structure at extreme levels appropriately. In certain applications, one would expect the extremes to occur simultaneously – a situation termed asymptotic dependence – whilst in others, joint occurrence of the very largest events cannot happen – a situation termed asymptotic independence. Section 2 explains these concepts in detail. The study of extremal dependence structures is well established, and a wide range of statistical modelling techniques have been proposed (Coles and Tawn, 1991; Ledford and Tawn, 1997; Heffernan and Tawn, 2004).

Extremal dependence between two variables may be summarised by bivariate risk measures. A variety of risk measures have been proposed in the literature (Serinaldi, 2015), and are selected according to the needs of an analysis. For this paper, we restrict attention to one particular measure known as the return curve due to its practical importance (Murphy-Barltrop et al., 2021). Given a small probability p , the p -probability return curve is given by $\text{RC}(p) := \{(x, y) \in \mathbb{R}^2 \mid \Pr(X > x, Y > y) = p\}$, with corresponding return period $1/p$. This curve directly extends the concept of a return level from the univariate framework (Coles, 2001) to the bivariate setting. These curves are widely used in practice to derive extremal conditions during the design analysis of many ocean and coastal structures, including oil rigs (Jonathan et al., 2014a), railway lines (Gouldby et al., 2017) and wind turbines (Manuel et al., 2018).

However, in many real world scenarios, datasets exhibit non-stationarity; this feature can result in extremal dependence structures that are not fixed due to covariate influences on the underlying processes. In this setting, there is no longer a meaningful or fixed

definition of a return curve. We therefore expand the definition of this risk measure to be covariate-dependent, resulting in a non-stationary counterpart. Given a process $\{X_t, Y_t\}$ with covariates \mathbf{Z}_t , $t \in \{1, 2, \dots, n\}$, we define the p -probability return curve at a covariate realisation \mathbf{z}_t to be $\text{RC}_{\mathbf{z}_t}(p) := \{(x, y) \in \mathbb{R}^2 \mid \Pr(X_t > x, Y_t > y \mid \mathbf{Z}_t = \mathbf{z}_t) = p\}$.

In a practical setting, we wish to derive estimates of non-stationary return curves for environmental datasets. As our motivating example, we consider relative humidity and temperature data for summer months (June, July and August) obtained from the UK Climate Projections (UKCP18) under emissions scenario RCP 8.5. This corresponds to the ‘worst-case’ scenario, whereby greenhouse gas emissions continue to rise throughout the 21st century (UK Met Office, 2018). As such, data from these projections can be used as a risk management tool to help mitigate against the impacts of climate change in a conservative manner. Data is only considered for summer months since extremal dependence structures vary significantly across meteorological seasons; see the Supplementary Material for further details.

Our particular dataset corresponds to temperature and relative humidity projections at a grid cell containing the UK’s Heysham nuclear power station. Denoting relative humidity by $\text{RH}_t \in [0, 100]$ for $t \in \{1, 2, \dots, n\}$, we define a ‘dryness’ variable as $\text{Dr}_t := 100 - \text{RH}_t \in [0, 100]$. The dataset of temperature and dryness at the start and end of the time period, along with the temperature time series, are plotted in the left and centre panels of Figure 1, respectively. Extremely high temperatures combined with extremely low humidity (i.e., high dryness) is relevant in the context of nuclear safety (Knochenhauer and Louko, 2004), and therefore one may wish to use these projections to quantify the joint extremal behaviour over the observation period. This dataset provides the subject of our detailed case study in Section 5. Clear non-stationary trends can be observed within both marginal data sets; these trends are likely a result of seasonal behaviour combined with long term trends due to climate change.

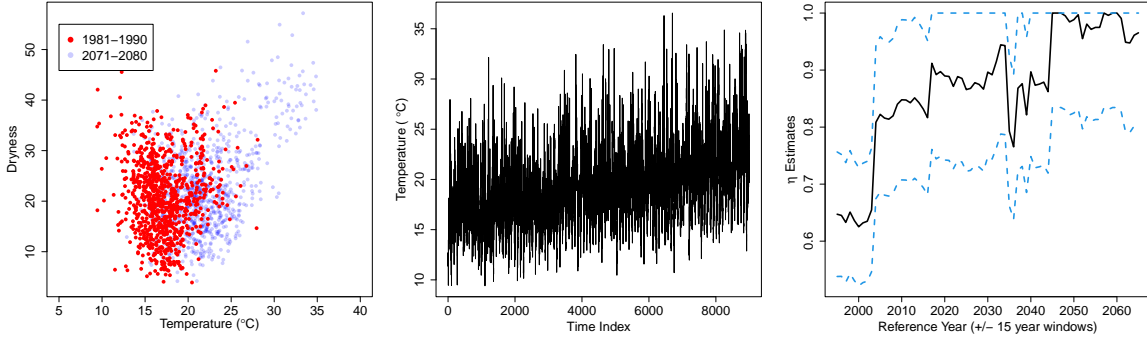


Figure 1: Left: Plot of first and last 10 years of combined temperature projections, given in red and light blue, respectively. Centre: Plot of Heysham temperature time series. Right: Plot of η estimates over rolling windows (solid black lines), alongside 95% pointwise confidence intervals (dotted blue lines).

To assess trends in dependence, we can calculate suitable coefficients using rolling windows of data. The right panel of Figure 1 demonstrates a clear trend in an extremal dependence coefficient labelled η (Ledford and Tawn, 1996); this measure summarises the dependence between the most extreme observations, with larger values corresponding to a higher degree of positive dependence. Further discussion can be found in Section 2.2. The illustrated trend suggests the probability of extreme observations occurring simultaneously is increasing over time, motivating the need for modelling techniques that can capture trends of this nature.

The majority of existing techniques for modelling multivariate extremes assume stationarity in the joint tail structure. Furthermore, of the approaches that can accommodate non-stationarity, most are suitable only for datasets exhibiting asymptotic dependence, as we discuss in Section 2.3. This is restrictive since in practice, asymptotic independence is often observed (Ledford and Tawn, 1996, 1997); this is further evidenced by estimated η values for the UKCP18 dataset, which indicate the presence of asymptotic independence, at least throughout most of the observation period.

We propose a new method for capturing non-stationary extremal dependence structures when asymptotic independence is present, based on a non-stationary extension to the Wadsworth and Tawn (2013) modelling framework. In doing so, we are able to evaluate and visualise trends across the entire extremal dependence structure. This is in contrast to other approaches, where implementation may be limited to trends in one-dimensional summary measures, such as the coefficient of tail dependence (Ledford and Tawn, 1996) or the extremal coefficient (Frahm, 2006).

This paper is structured as follows: Section 2 recalls existing methodology for capturing tail behaviour in the stationary and non-stationary settings for both univariate and multivariate random vectors. Section 3 introduces our modelling approach, which relies on quantile regression techniques to derive two estimators of a quantity describing extremal dependence in a non-stationary setting. We also propose methodology for non-stationary return curve estimation using these estimators. Section 4 details a simulation study, showing our estimators to be approximately unbiased over a range of simulated examples. In Section 5, we apply our model to the UKCP18 dataset. Our approach is able to reveal clear trends in the extremal dependence of this process, and estimates of return curves are obtained. We conclude in Section 6 with a discussion and outlook on future work.

2 Background

2.1 Univariate extreme value theory

In the univariate setting, one of the most popular techniques for capturing tail behaviour is known as the peaks-over-threshold approach, whereby a generalised Pareto distribution (GPD) is fitted to all exceedances of some high threshold. This is justified by the Pickands-Balkema-de Haan theorem (Balkema and de Haan, 1974; Pickands, 1975), which states that for a random variable X satisfying certain regularity conditions, there exists a normalising

function $c(u)$ such that

$$\Pr\left(\frac{X-u}{c(u)} \leq x \mid X > u\right) \rightarrow G(x) := 1 - \left\{1 + \frac{\xi x}{\tau}\right\}_+^{-1/\xi}, \quad x > 0, (\tau, \xi) \in \mathbb{R}^+ \times \mathbb{R}, \quad (2.1)$$

as $u \rightarrow x^F := \sup\{x : F(x) < 1\}$; see also Coles (2001). Here, $G(x)$ is the cumulative distribution function of a GPD, with scale and shape parameters, τ and ξ , respectively, and $z_+ = \max(0, z)$. The shape parameter dictates the behaviour of the tail, with $\xi < 0$, $\xi = 0$ and $\xi > 0$ corresponding to bounded, exponential and heavy tails, respectively. In practice, for an observed random variable with a finite sample size, a high threshold u is selected and a GPD is fitted to the positive exceedances: we write $X - u \mid X > u \sim \text{GPD}(\tau, \xi)$.

In many contexts, such as financial and environmental modelling, datasets exhibit non-stationarity, whereby the underlying distribution changes with time or other covariates. In most such cases, we can no longer expect a stationary GPD model to capture the tail adequately. This feature can be present in a range of different forms, as exhibited by the seasonal and long term trends present in the UKCP18 dataset introduced in Section 1. Davison and Smith (1990) addressed this issue by using covariates to capture trends in the GPD parameters. Given a non-stationary process $\{Y_t\}$, with covariates \mathbf{Z}_t , a non-stationary GPD model is given by

$$(Y_t - u \mid Y_t > u, \mathbf{Z}_t = \mathbf{z}_t) \sim \text{GP}(\tau(\mathbf{z}_t), \xi(\mathbf{z}_t)), \quad (2.2)$$

for a sufficiently large threshold u . More recent extensions to this model also allow the threshold u to be covariate dependent. For example, Kysely et al. (2010) and Northrop and Jonathan (2011) use quantile regression to estimate a threshold with a constant exceedance probability, whereas Sigauke and Bere (2017) use a cubic smoothing spline. More flexible approaches have been proposed using generalised additive models (GAMs) to capture non-stationary behaviour in univariate extremes (Chavez-Demoulin and Davison, 2005; Youngman, 2019). GAMs use smooth functions to capture trends due to covariates, and are

less rigid than standard regression models. A wide range of statistical software is available for fitting these models (Youngman, 2020; Wood, 2021).

All the approaches discussed thus far can only be used to model non-stationarity in the extremes. For many statistics corresponding to joint tail behaviour, such as return curves, one must also be able to capture non-stationarity within the body of the data simultaneously. This is because extremes of one variable may occur with average values of another variable. To address such challenges, a range of pre-processing techniques have been proposed that allow marginal non-stationarity to be captured in the body and tail of a dataset simultaneously (Nogaj et al., 2007; Eastoe and Tawn, 2009; Mentaschi et al., 2016). For these approaches, covariate functions are used to capture and effectively ‘remove’ non-stationarity from the body of the data. Once removed, any remaining trends in the tail can be captured using any of the methods introduced above. For a non-stationary process $\{Y_t\}$, with covariates \mathbf{Z}_t , the general set-up of these models is to assume

$$(Y_t | \mathbf{Z}_t = \mathbf{z}_t) = \mu(\mathbf{z}_t) + \sigma(\mathbf{z}_t)R_t, \quad (2.3)$$

with μ and $\log(\sigma)$ as linear functions of covariates. Here, the residual process $\{R_t\}$ is assumed to be approximately stationary, and assigning a distribution to this yields a likelihood for all parameters; Eastoe and Tawn (2009), for example, adopt a standard normal distribution, with the option to also include a shape transformation. Covariate functions are selected through an analysis of non-stationary trends within the body.

An alternative is given by Krock et al. (2021), who propose a single distribution for capturing non-stationary behaviour in the body and tail simultaneously. This distribution, which extends the model for stationary data proposed in Stein (2021), accounts for both seasonal and long term trends. The idea behind this approach is to provide a ‘one size fits all’ model, hence the same trends are assumed to be present within the extremes as in the rest of the data. This is unlikely to be the case in all practical scenarios; as a result, we

prefer to adopt pre-processing techniques.

2.2 Bivariate extreme value theory

We briefly recall approaches to modelling extremes in the bivariate setting. To begin, consider a random vector (X, Y) with respective marginal distribution functions F_X, F_Y . Consider the conditional probability $\chi(u) = \Pr(F_Y(Y) > u \mid F_X(X) > u)$ and define the coefficient $\chi := \lim_{u \rightarrow 1} \chi(u) \in [0, 1]$. The cases $\chi = 0$ and $\chi > 0$ correspond to the aforementioned asymptotic independence and asymptotic dependence schemes, respectively. This distinction is important since many models are suitable for data exhibiting one scheme only.

For mathematical simplicity in the description of extremal dependence, it is common to consider random vectors with standardised marginal distributions. This is achieved in practice through marginal estimation and application of the probability integral transform.

Classical modelling approaches are based on the framework of multivariate regular variation, and are applicable only to asymptotically dependent data. Given a random vector (X, Y) with standard Fréchet margins, we define the radial and angular components to be $R := X + Y$ and $W := X/R$, respectively. We say that (X, Y) is multivariate regularly varying if, for all Borel subsets $B \in [0, 1]$, we have

$$\lim_{r \rightarrow \infty} \Pr(W \in B, R > sr \mid R > r) = H(B)s^{-1},$$

for any $s > 1$, where H is termed the spectral measure (Resnick, 1987). This assumption implies that, for large radial values, R and W are independent. The spectral measure captures the extremal dependence structure of (X, Y) . It must satisfy the moment constraint $\int_0^1 wH(dw) = 1/2$, but has no closed parametric form. All asymptotically independent distributions have a spectral measure placing mass at the endpoints $\{0\}$ and $\{1\}$ of the unit interval, which is why this modelling framework is unable to capture tail properties

under this scheme (Coles et al., 1999). Moreover, it has been shown that assuming the incorrect form of extremal dependence will lead to unsatisfactory extrapolation in the joint tail (Ledford and Tawn, 1997; Heffernan and Tawn, 2004). This has consequently led to the development of flexible modelling approaches that are able to theoretically capture both extremal dependence regimes.

The first such idea was proposed in Ledford and Tawn (1996, 1997). It is assumed that the joint tail of a random vector (X, Y) with standard exponential margins is given by

$$\Pr(X > u, Y > u) = \Pr(\min(X, Y) > u) = L(e^u)e^{-u/\eta} \text{ as } u \rightarrow \infty, \quad (2.4)$$

where L is a slowly varying function at infinity, i.e., $\lim_{x \rightarrow \infty} L(cx)/L(x) = 1$ for $c > 0$, and $\eta \in (0, 1]$. The parameter η is termed the coefficient of tail dependence, with $\eta = 1$ and $\lim_{u \rightarrow \infty} L(e^u) > 0$ corresponding to asymptotic dependence and $\eta < 1$, or $\eta = 1$ and $\lim_{u \rightarrow \infty} L(e^u) = 0$, corresponding to asymptotic independence. In Figure 1, our estimates of η suggest asymptotic independence is exhibited by the UKCP18 data throughout most of the observation period. In practice, this framework is limited by the fact it only characterises the joint tail where both variables are large, and hence is not applicable in regions where only one variable is extreme.

Alternative characterisations of the joint tail have been proposed to circumvent this issue. Heffernan and Tawn (2004) introduce a general, regression-based modelling tool for conditional probabilities. Given a random vector (X, Y) with standard Laplace margins (Keef et al., 2013), it is assumed that normalising functions $a : \mathbb{R} \rightarrow \mathbb{R}$ and $b : \mathbb{R} \rightarrow (0, \infty)$ exist such that the following convergence holds:

$$\lim_{u \rightarrow \infty} \Pr [(Y - a(X))/b(X) \leq z, X - u > x \mid X > u] = D(z)e^{-x}, \quad x > 0,$$

for a non-degenerate distribution function D . Both regimes can be captured via the functions a and b , with asymptotic dependence arising when $a(x) = x$ and $b(x) = 1$. Note that

one could instead condition on the event $Y > u$. The functions a and b are typically estimated parametrically, while the distribution function D is estimated non-parametrically. This model has been widely used in practice, with applications ranging from ocean engineering (Ross et al., 2020) to coastal flood mitigation (Gouldby et al., 2017).

Wadsworth and Tawn (2013) provide an alternative representation for the joint tail using a general extension of the framework described in equation (2.4). Given (X, Y) with standard exponential margins, they assume that for each $w \in [0, 1]$,

$$\Pr(\min\{X/w, Y/(1-w)\} > u) = L(e^u; w)e^{-\lambda(w)u}, \quad \lambda(w) \geq \max(w, 1-w), \quad (2.5)$$

as $u \rightarrow \infty$, where $L(\cdot; w)$ is slowly varying for each ray $w \in [0, 1]$ and λ is termed the angular dependence function (ADF). This function, which describes the dependence structure of the joint tail along the ray w , generalises the coefficient η , with $\eta = 1/\{2\lambda(0.5)\}$. Both extremal dependence regimes can be captured by λ , with asymptotic dependence implying the lower bound $\lambda(w) = \max(w, 1-w)$ for all $w \in [0, 1]$. Pointwise estimates of the ADF can be obtained in practice via the Hill estimator (Hill, 1975).

Alongside these approaches, we note that there exist several copula-based models that can theoretically capture both extremal dependence regimes, such as those given in Pauli and Coles (2002), Wadsworth et al. (2017) and Huser and Wadsworth (2019). However, due to the stronger assumptions about the form of parametric family for the bivariate distribution, we prefer instead to use more flexible modelling techniques.

2.3 Non-stationary extremal dependence

Although many extreme value analyses seek to capture marginal non-stationarity, common practice is to assume stationarity in dependence, often without even assessing this feature. Relatively little consideration has been given to this problem in the literature, and most of the approaches that do exist rely on the multivariate regular variation framework,

thereby being restricted to asymptotically dependent data. For example, Mhalla et al. (2019a) and Mhalla et al. (2019b) propose semi-parametric models to capture trends in parameters of quantities related to the spectral measure, while de Carvalho and Davison (2014) and Castro-Camilo et al. (2018) propose flexible modelling techniques for capturing non-stationary trends in the spectral measure under covariate influence.

Mhalla et al. (2019) also propose a technique for data exhibiting asymptotic independence, using GAMs to capture trends in the non-stationary extension to the ADF defined in equation (3.1). Given a non-stationary process $\{X_t, Y_t\}$ with standard exponential margins and an external p -dimensional covariate \mathbf{Z}_t , the extended ADF $\lambda(\cdot : \mathbf{Z}_t = \mathbf{z}_t)$ is assumed to take the semi-parametric form

$$\lambda(w : \mathbf{Z}_t = \mathbf{z}_t, \boldsymbol{\phi}) = h_w^{-1} \left\{ (\mathbf{z}_t^1)' \boldsymbol{\gamma} + \sum_{a=1}^A s^a(\mathbf{z}_{t,a}^2) \right\}, \quad (2.6)$$

where h_w is a link function, and $\mathbf{z}_t^1, \mathbf{z}_{t,1}^2, \dots, \mathbf{z}_{t,A}^2$ are subvectors of \mathbf{z}_t , or products of covariates if interactions are considered. The vector $\boldsymbol{\gamma}$ gathers linear coefficients whereas s^a denote smooth functions for each $a \leq A$; the parameter vector $\boldsymbol{\phi}$ represents all parameters to be estimated, i.e., $\boldsymbol{\gamma}$ and the coefficients from each basis function s^a . Estimation of $\boldsymbol{\phi}$ is via a penalised log-likelihood approach, where roughness penalties are imposed to ensure a smooth model fit. The link function $h_w(x) = \log\{[x - \max(w, 1 - w)] / (1 - x)\}$ is used, resulting in fitted values contained in the interval $[\max(w, 1 - w), 1]$. However, this range is restrictive since $\lambda(w) \leq 1$ implies positive extremal association. In practice, Mhalla et al. (2019) only applied model (2.6) along the ray $w = 1/2$, corresponding to modelling non-stationarity in η only. In Section 3, we propose a novel modelling framework for capturing extremal dependence trends under asymptotic independence via a non-stationary extension to the ADF. A simulation study in Section 4 demonstrates that our approach often results in less bias and variability compared to the technique given in Mhalla et al. (2019).

Non-stationary extensions to the Heffernan and Tawn (2004) model also exist: Jonathan et al. (2014b) propose smooth covariate functions for a and b , while Guerrero et al. (2021) allow these parameters to vary smoothly over time for blocks of observations via a penalised log-likelihood. However, we note that conditional extremes techniques have been shown to create additional complexities during implementation, requiring more steps compared to alternative approaches because of the need to condition on each variable being extreme separately; see Murphy-Barltrop et al. (2021). Our proposed method is simpler to implement in practice compared to the those derived under this framework.

3 Non-stationary angular dependence function

3.1 Introduction

We describe a non-stationary extension to the ADF λ of Wadsworth and Tawn (2013), which is the key building block for estimating non-stationary return curves. We assume stationary marginal distributions throughout this section, allowing us to separate out the two forms of trends; further discussion on the separate treatment of these trends can be found in Section 5.

Given a non-stationary process $\{X_t, Y_t\}$ with standard exponential margins and an external p -dimensional covariate \mathbf{Z}_t , we assume that for all $w \in [0, 1]$ and $t \in \{1, 2, \dots, n\}$,

$$\Pr \left(\min \left\{ \frac{X_t}{w}, \frac{Y_t}{1-w} \right\} > u \mid \mathbf{Z}_t = \mathbf{z}_t \right) = L(e^u \mid w, \mathbf{Z}_t = \mathbf{z}_t) e^{-\lambda(w \mid \mathbf{Z}_t = \mathbf{z}_t)u} \text{ as } u \rightarrow \infty, \quad (3.1)$$

where L denotes a slowly varying function and $\lambda(\cdot \mid \mathbf{Z}_t = \mathbf{z}_t)$ denotes the non-stationary counterpart of the ADF at time t . Define $K_{w,t} := \min \{X_t/w, Y_t/(1-w)\}$: we refer to this variable as the min-projection. Equation (3.1) implies that, for each $w \in [0, 1]$, and $t \leq n$,

$$\Pr \left(K_{w,t} > v + u \mid K_{w,t} > u, \mathbf{Z}_t = \mathbf{z}_t \right) \rightarrow \exp\{-v\lambda(w \mid \mathbf{Z}_t = \mathbf{z}_t)\} \text{ as } u \rightarrow \infty, \quad v > 0.$$

However, unlike its stationary counterpart, the non-stationary ADF cannot be estimated via the Hill estimator; this is because we typically do not have repeated observations for a covariate realisation. Moreover, even with repeated observations, the resulting sample sizes would typically be too small for reliable estimation. As such, a new estimation procedure is required for this function. Given $w \in [0, 1]$ and two quantiles q_1, q_2 close to one with $q_1 < q_2 < 1$, we assume the existence of positive sequences $\{u_{w,t}\}_{t \leq n}$ and $\{v_{w,t}\}_{t \leq n}$ such that

$$\Pr(K_{w,t} \leq u_{w,t} \mid \mathbf{Z}_t = \mathbf{z}_t) = q_1, \quad \Pr(K_{w,t} \leq u_{w,t} + v_{w,t} \mid \mathbf{Z}_t = \mathbf{z}_t) = q_2, \quad (3.2)$$

for all $t \leq n$. Assuming strict monotonicity of the cumulative distribution function for $K_{w,t} \mid (\mathbf{Z}_t = \mathbf{z}_t)$, we deduce that $v_{w,t} > 0$ for all $t \leq n$. Furthermore, the quantile q_1 being close to one implies values of the sequence $\{u_{w,t}\}_{t \leq n}$ are large in magnitude. Under the model assumptions, we can therefore deduce that

$$\frac{1 - q_2}{1 - q_1} = \Pr\left(K_{w,t} > v_{w,t} + u_{w,t} \mid K_{w,t} > u_{w,t}, \mathbf{Z}_t = \mathbf{z}_t\right) \approx \exp\{-v_{w,t}\lambda(w \mid \mathbf{Z}_t = \mathbf{z}_t)\},$$

which is rearranged to give

$$\lambda(w \mid \mathbf{Z}_t = \mathbf{z}_t) \approx -\frac{1}{v_{w,t}} \log\left(\frac{1 - q_2}{1 - q_1}\right), \quad (3.3)$$

for all $t \leq n$. Hence, estimates of the sequence $\{v_{w,t}\}_{t \leq n}$ lead to a point-wise estimator for the non-stationary ADF at a given angle $w \in [0, 1]$. We denote this estimator by $\hat{\lambda}(\cdot \mid \mathbf{z}_t)$, and describe improvements to its stability in Section 3.3.

3.2 Estimating quantiles of the min-projection

The sequence $\{v_{w,t}\}_{t \leq n}$ corresponds to differences in covariate-varying quantiles of the univariate min-projection $K_{w,t} \mid (\mathbf{Z}_t = \mathbf{z}_t)$ for each $w \in [0, 1]$. Quantile regression methods therefore provide a natural solution to the problem of its estimation. Such techniques have successfully been applied in a variety of contexts, ranging from ecology (Cade and Noon,

2003) to growth charts (Wei et al., 2006). Here, we describe the most commonly-used approach in terms of the min-projection variable. Given a value $q \in (0, 1)$, the q -th quantile of $K_{w,t} \mid (\mathbf{Z}_t = \mathbf{z}_t) \sim F_{K_{w,t} \mid \mathbf{z}_t}$ is

$$Q_{K_{w,t} \mid (\mathbf{z}_t = \mathbf{z}_t)}(q) = \inf\{x : F_{K_{w,t} \mid \mathbf{z}_t}(x \mid \mathbf{z}_t) \geq q\}.$$

We assume that the conditional quantile function is linear in \mathbf{z}_t , implying $Q_{K_{w,t} \mid (\mathbf{z}_t = \mathbf{z}_t)}(q) = \mathbf{z}_t' \boldsymbol{\pi}$, where $\boldsymbol{\pi} \in \mathbb{R}^p$ denotes a vector of coefficients. The vector $\boldsymbol{\pi}$ is estimated through a minimisation of a suitable loss function; see Koenker et al. (2017) for further details.

There is also a range of literature available on the topic of extremal quantile regression (Chernozhukov, 2004; Youngman, 2019; Velthoen et al., 2021), applicable when q is very close to one. However, many of the derived extreme value laws involve unknown constants which cannot be estimated without strong modelling assumptions (Chernozhukov et al., 2017). Furthermore, applying the simple ‘rule-of-thumb’ proposed in Chernozhukov and Fernández-Val (2011) for deciding between extreme value and normal quantile approximations, the quantile levels considered in Sections 4 and 5 would not be deemed extreme enough to warrant the former. Moreover, we have found standard quantile regression techniques are able to produce accurate estimates of non-stationary ADFs across a range of simulated examples.

3.3 Averaging over quantiles

Prior to applying the proposed model, one must first select q_1 and q_2 for estimating quantiles of $K_{w,t}$. This selection represents a bias-variance trade off, as is often observed in applications of extreme value theory: quantiles that are not sufficiently extreme (close to one) will induce bias in results, while quantiles that are too large will result in highly variable estimates. Moreover, considering only a single pair of quantiles will lead to higher variability in ADF estimates. To address these issues, we consider a range of quantile

pairs simultaneously and compute an average estimator over these values. Specifically, let $\{(q_{1,j}, q_{2,j}) \mid 1 \leq j \leq m\}$ be quantiles near one, with $q_{1,j} < q_{2,j} < 1$ for $j = 1, \dots, m$. For each j , the pair $(q_{1,j}, q_{2,j})$ is used to derive an estimator $\hat{\lambda}_j$, as in equation (3.3). Our final estimator is derived to be the average of these:

$$\bar{\lambda}_{QR}(w \mid \mathbf{z}_t) := \frac{1}{m} \sum_{j=1}^m \hat{\lambda}_j(w \mid \mathbf{z}_t),$$

for all $w \in [0, 1]$ and $t \leq n$. In unreported simulations, we have found this aggregated estimator to outperform estimators obtained from any individual pair of quantiles considered. Furthermore, a range of quantile sets were compared for the examples discussed in Section 4, with the resulting ADF estimates showing very little difference in variability or accuracy. Our choices for m and $\{(q_{1,j}, q_{2,j})\}$ are detailed in Section 4.

3.4 Bernstein-Bézier polynomial smooth estimator

One drawback of the average estimator $\bar{\lambda}_{QR}$ proposed in Section 3.3 is that it is pointwise for each ray $w \in [0, 1]$. This typically leads to non-smooth estimates of the ADF that one would not expect to observe in practice.

In this section, we extend this estimator to give smooth functional estimates using a parametric family derived from the set of Bernstein-Bézier polynomials. These polynomials have been applied in many approaches to estimate Pickands dependence function (Guillotte and Perron, 2016; Marcon et al., 2016, 2017), a quantity related to the spectral measure which bears many similarities to the ADF (Wadsworth and Tawn, 2013). For dimension $d = 2$, the family of Bernstein-Bézier polynomials of degree $k \in \mathbb{N}$ is defined to be

$$\mathcal{B}_k = \left\{ \sum_{i=0}^k \alpha_i \binom{k}{i} w^i (1-w)^{k-i} : \boldsymbol{\alpha} \in [0, 1]^{k+1}, w \in [0, 1] \right\}.$$

We use this family of functions to approximate $\lambda(\cdot \mid \mathbf{Z}_t = \mathbf{z}_t)$. However, for any $f \in \mathcal{B}_k$, we have $f(w) \leq 1$ for all $w \in [0, 1]$. As such, this family of polynomials can only

approximate ADFs representing non-negative dependence in the extremes. Furthermore, we wish to allow for covariate influence in the dependence structure; this corresponds to covariate influence in the coefficient vector $\boldsymbol{\alpha}$. We therefore propose extending this family of polynomials to the following set:

$$\mathcal{B}_k^* \mid (\mathbf{Z}_t = \mathbf{z}_t) = \left\{ \sum_{i=0}^k \beta_i(\mathbf{z}_t) \binom{k}{i} w^i (1-w)^{k-i} : \boldsymbol{\beta}(\mathbf{z}_t) \in [0, \infty)^{k+1}, w \in [0, 1] \right\},$$

where $\beta_i : \mathbb{R}^p \rightarrow [0, \infty)$ denote functions of the covariates. For any $t \leq n$, let $\lambda_{BP}(\cdot \mid \mathbf{z}_t) \in \mathcal{B}_k^* \mid (\mathbf{Z}_t = \mathbf{z}_t)$ represent a form of the non-stationary ADF given by this family of functions. Our objective is to find an estimator $\bar{\lambda}_{BP}$ that minimises the equation

$$|\lambda(w \mid \mathbf{Z}_t = \mathbf{z}_t) - \lambda_{BP}(w \mid \mathbf{z}_t)| \quad (3.4)$$

over all rays $w \in [0, 1]$ and \mathbf{z}_t for $t \leq n$; this is achieved through estimation of the coefficient functions β_i . Since λ is unobserved in practice, we consider the objective function

$$S(\boldsymbol{\theta}) := \frac{1}{|\mathcal{W}|n} \sum_{w \in \mathcal{W}} \sum_{t=1}^n |\bar{\lambda}_{QR}(w \mid \mathbf{z}_t) - \lambda_{BP}(w \mid \mathbf{z}_t, \boldsymbol{\theta})|, \quad (3.5)$$

with $\mathcal{W} := \{0, 0.01, 0.02, \dots, 0.99, 1\}$ defining a finite set spanning the interval $[0, 1]$ and $\boldsymbol{\theta}$ denoting the parameter vector corresponding to the coefficient functions $\{\beta_0, \beta_1, \dots, \beta_k\}$. The intuition here is that $S(\boldsymbol{\theta})$ gives an approximation of the absolute value in (3.4) integrated over w and t : it is therefore desirable to find a value of $\boldsymbol{\theta}$ which minimises S .

To estimate $\boldsymbol{\theta}$, we must specify the form of coefficient functions. To start, we impose that $\beta_0(\mathbf{z}_t) = \beta_k(\mathbf{z}_t) = 1$ for all $t \leq n$; any function $f \in \mathcal{B}_k^* \mid (\mathbf{Z}_t = \mathbf{z}_t)$ satisfying these conditions has the property that $f(0) = f(1) = 1$, corresponding to the theoretical end-points of the ADF: $\lambda(0) = \lambda(1) = 1$. For $i \in \{1, 2, \dots, k-1\}$, we assume that $\beta_i(\mathbf{z}_t) = h(\mathbf{z}_t' \boldsymbol{\theta}_i)$, where $h : \mathbb{R} \rightarrow [0, \infty)$ denotes a link-function and $\boldsymbol{\theta}_i \in \mathbb{R}^p$ denotes a vector of coefficients for each i . The entire parameter vector is therefore $\boldsymbol{\theta} := \{\boldsymbol{\theta}_1, \boldsymbol{\theta}_2, \dots, \boldsymbol{\theta}_{k-1}\}$, with an estimator defined as

$$\hat{\boldsymbol{\theta}} = \arg \min_{\boldsymbol{\theta} \in \mathbb{R}^{p(k-2)}} S(\boldsymbol{\theta}).$$

Finally, a smooth estimator of $\lambda(\cdot \mid \mathbf{Z}_t = \mathbf{z}_t)$ is given by $\bar{\lambda}_{BP}(\cdot \mid \mathbf{z}_t) := \lambda_{BP}(\cdot \mid \mathbf{z}_t, \boldsymbol{\theta} = \hat{\boldsymbol{\theta}})$.

3.5 Incorporating theoretical properties

Wadsworth and Tawn (2013) show that the ADF is bounded from below, i.e, $\lambda(w) \geq \max(w, 1 - w)$ for all $w \in [0, 1]$. This bound corresponds to asymptotic dependence, with larger values corresponding to a form of asymptotic independence. Neither of our estimators $\bar{\lambda}_{QR}$ or $\bar{\lambda}_{BP}$ are required to satisfy this constraint, and so we impose this bound retrospectively. In each case, we define $\bar{\lambda}_{QR}^*$ or $\bar{\lambda}_{BP}^*$ as

$$\bar{\lambda}_{QR}^*(w \mid \mathbf{z}_t) = \max \left\{ \bar{\lambda}_{QR}(w \mid \mathbf{z}_t), \max(w, 1 - w) \right\},$$

for all $w \in [0, 1]$, and similarly for $\bar{\lambda}_{BP}^*$. In unreported results, we found that incorporating this lower bound improves estimation quality within the resulting ADF estimates.

For $\bar{\lambda}_{QR}^*$, we also impose end-point conditions retrospectively: $\bar{\lambda}_{QR}^*(0 \mid \mathbf{Z}_t = \mathbf{z}_t) = \bar{\lambda}_{QR}^*(1 \mid \mathbf{Z}_t = \mathbf{z}_t) = 1$ for all $t \leq n$. Recall that this requirement is already satisfied by the smooth estimator by setting $\beta_0(\mathbf{z}_t) = \beta_k(\mathbf{z}_t) = 1$ for all $t \leq n$.

3.6 Estimating non-stationary return curves

We now consider the problem of estimating $\text{RC}_{\mathbf{z}_t}(p)$ at some fixed $t \leq n$ using an estimator of the non-stationary ADF. Let λ^* denote either the estimator $\bar{\lambda}_{QR}^*$ or $\bar{\lambda}_{BP}^*$. Given the set of rays \mathcal{W} defined in Section 3.4 and a quantile q_1 close to one, we let $\{u_{w,t}\}_{w \in \mathcal{W}}$ be defined as in equation (3.2). Then, for all $w \in \mathcal{W}$, define $\{r_{w,t}\}_{w \in \mathcal{W}}$ as

$$r_{w,t} := -\frac{1}{\lambda^*(w \mid \mathbf{z}_t)} \log \left(\frac{p}{1 - q_1} \right),$$

implying $\frac{p}{1-q_1} = \exp\{-r_{w,t}\lambda^*(w \mid \mathbf{z}_t)\} \approx \exp\{-r_{w,t}\lambda(w \mid \mathbf{Z}_t = \mathbf{z}_t)\}$. Define $(x_{w,t}, y_{w,t}) := (w(r_{w,t} + u_{w,t}), (1-w)(r_{w,t} + u_{w,t}))$. We have

$$\begin{aligned}
\Pr(X_t > x_{w,t}, Y_t > y_{w,t} \mid \mathbf{Z}_t = \mathbf{z}_t) &= \Pr(K_{w,t} > r_{w,t} + u_{w,t} \mid \mathbf{Z}_t = \mathbf{z}_t) \\
&= \Pr(K_{w,t} > r_{w,t} + u_{w,t} \mid K_{w,t} > u_{w,t}, \mathbf{Z}_t = \mathbf{z}_t) \\
&\quad \times \Pr(K_{w,t} > u_{w,t} \mid \mathbf{Z}_t = \mathbf{z}_t) \\
&\approx \exp\{-r_{w,t}\lambda^*(w \mid \mathbf{z}_t)\} \Pr(K_{w,t} > u_{w,t} \mid \mathbf{Z}_t = \mathbf{z}_t) \\
&= \frac{p}{1-q_1} \times 1 - q_1 = p,
\end{aligned}$$

meaning that the set $\{(x_{w,t}, y_{w,t})\}_{w \in \mathcal{W}}$ provides an approximation of $\text{RC}_{\mathbf{z}_t}(p)$. Similarly to the estimation of $\bar{\lambda}_{QR}^*$ and $\bar{\lambda}_{BP}^*$, as described in Sections 3.3 and 3.4, we denote $\widehat{\text{RC}}_{\mathbf{z}_t}^j(p) = \{(x_{w,t}^j, y_{w,t}^j)\}_{w \in \mathcal{W}}$ for each quantile $q_{1,j}$ close to one, and take our final estimator of the return curve to be $\overline{\text{RC}}_{\mathbf{z}_t}(p) = \{(\sum_{j=1}^m x_{w,t}^j/m, \sum_{j=1}^m y_{w,t}^j/m)\}_{w \in \mathcal{W}}$.

4 Simulation study

4.1 Overview

We use simulation to evaluate the properties of the estimators $\bar{\lambda}_{QR}^*$ and $\bar{\lambda}_{BP}^*$ derived in Section 3. Section 4.2 introduces a range of examples exhibiting non-stationary extremal dependence. The variation in dependence structures allows us to assess the relative strengths and weaknesses of each estimator. In Section 4.3, we consider parametric forms for the covariate and link functions introduced in Section 3. In Section 4.4, we evaluate the bias and variability that arises from $\bar{\lambda}_{QR}^*$ and $\bar{\lambda}_{BP}^*$, which we find to outperform the corresponding estimator from Mhalla et al. (2019). To the best of our knowledge, these are the only approaches within the literature for capturing trends in extremal dependence under asymptotic independence. Finally, in Section 4.5, we illustrate that our proposed estimators can be used to derive accurate estimates of non-stationary return curves across each

of the considered examples.

4.2 Simulated examples of non-stationary dependence structures

We introduce several examples exhibiting non-stationary extremal dependence under asymptotic independence. In each case, the non-stationarity is over the time covariate $t \in \{1, 2, \dots, n\}$, with $n = 10,000$ denoting the sample size. The first two examples are obtained using the bivariate normal copula, for which the dependence is characterised by the coefficient $\rho \in [-1, 1]$. For the first example, we take $\rho(t) = t/n$, so that $\rho(0) = 0$ and $\rho(1) = 1$, i.e., moving from independence to perfect positive dependence. For the second example, we take $\rho(t) = -0.9 + 0.9t/n$, giving $\rho(0) = -0.9$ and $\rho(1) = 0$, i.e., moving from a strong negative correlation to independence.

For the third, fourth and fifth examples, we use the inverted extreme value copula (Ledford and Tawn, 1997) with logistic, asymmetric logistic and Hüsler-Reiss families, respectively. For the logistic and asymmetric logistic, the dependence is characterised by the parameter $r \in (0, 1)$, with the degree of positive dependence increasing as r approaches 0. We take $r(t) = 0.01 + 0.98t/n$, hence moving from strong positive dependence at $t = 0$ to close to independence at $t = n$. The asymmetric logistic distribution also requires two asymmetry parameters $(\kappa_1, \kappa_2) \in [0, 1]^2$ (Tawn, 1988): we fix $(\kappa_1, \kappa_2) = (0.3, 0.7)$, noting this does not change the overall trend in dependence. The Hüsler-Reiss family is characterised by the dependence parameter $s > 0$, with independence and complete dependence obtained as s approaches 0 and ∞ , respectively. We take $s(t) = 0.01 + 9.99t/n$, resulting in increasing dependence over time.

For the final example, we start with a specified ADF and use a method given in Nolde and Wadsworth (2021) to construct a copula with this ADF. Given the dependence parameter $c \in (0, 1)$, we take $\lambda(w) = \max\{(2w - 1)/c, (1 - 2w)/c, 1/(2 - c)\}$, which is the ADF

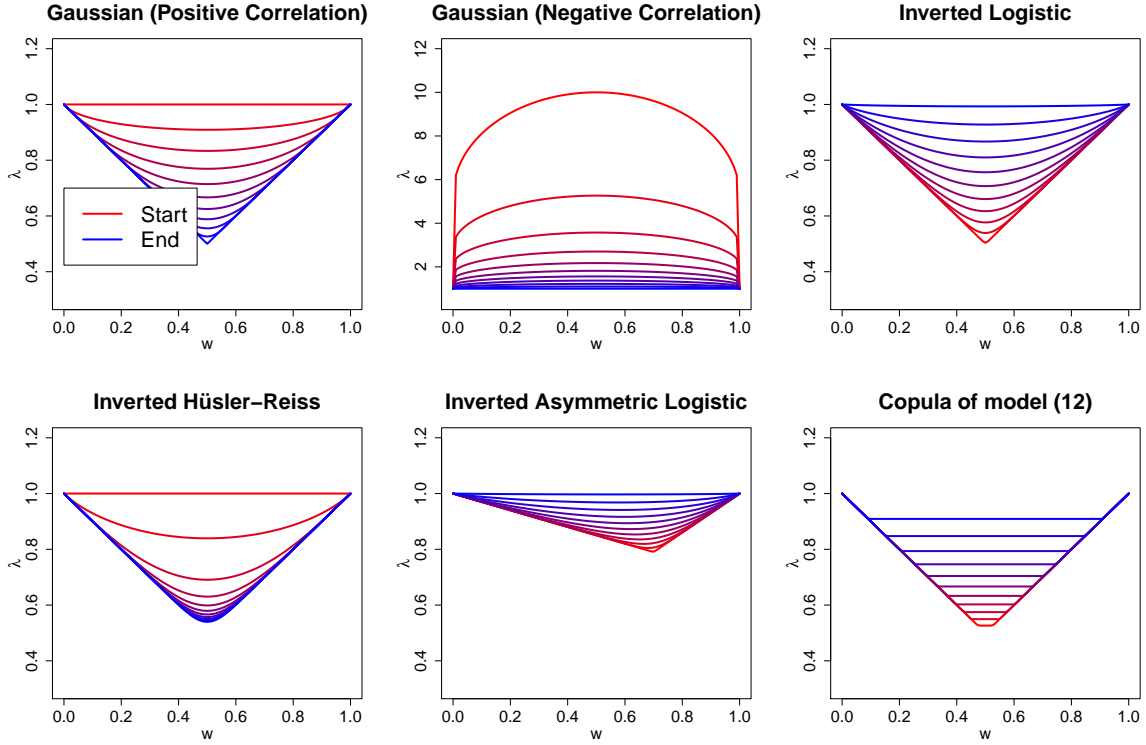


Figure 2: Illustration of true ADFs over time for each copula example. Colour change is used to illustrate trends in extremal dependence structure over the time frame, with red and blue corresponding to the start and end of time frame, respectively.

of the density proportional to

$$\exp(-\max\{(x-y)/c, (y-x)/c, (x+y)/(2-c)\}), \quad (4.1)$$

and simulate from this density using MCMC. Such a distribution does not have exactly exponential margins, however in this case the transformation to exponential margins, via the probability integral transform, yields a density with the same ADF. We refer to this example as the copula of model (4.1) henceforth and set $c(t) = 0.1 + 0.8t/n$; this results in a similar dependence trend to the inverted logistic example. Illustrations of the resulting ADFs over time for each example are given in Figure 2.

4.3 Covariate and link functions

Both estimators derived in Section 3 require estimates of sequences obtained via a quantile regression procedure. For this, one must first specify the functional form for the relationship between quantiles and covariates \mathbf{z}_t . Since the data we have simulated has a dependence structure directly related to the covariate t , we propose the covariate set $\mathbf{z}_t := \{1, t, t^2, t^3\}$. For any given quantile q and ray $w \in [0, 1]$, it is assumed that the quantile function is given by $Q_{K_{w,t}|\mathbf{z}_t=\mathbf{z}_t}(q) = \mathbf{z}'_t \boldsymbol{\pi}$, where $\boldsymbol{\pi} \in \mathbb{R}^4$. Additional polynomial terms were considered, but we found that a cubic expression was flexible enough to accurately capture quantiles trends for each of the studied examples. Applying the methodology described in Koenker et al. (2017), estimates of the sequences described in equation (3.2) can be obtained for any pair of quantiles q_1, q_2 .

As noted in Section 3.3, the choice of quantile sets did not appear to significantly alter the resulting ADF estimates, so long as a range of different quantile pairs were considered. Therefore, for $\{q_{1,j}\}_{j=1}^m$, we take $m = 30$ equally spaced points in the interval $[0.9, 0.95]$, and set $q_{2,j} = q_{1,j} + 0.04$ for $j = 1, \dots, m$.

For $\bar{\lambda}_{QR}^*$, estimates of non-stationary ADFs can be derived directly using estimated sequences, while specification of a coefficients functions is also required for $\bar{\lambda}_{BP}^*$. Defining $\mathbf{z}_t := \{1, t\}$, we set $\log(\beta_i(\mathbf{z}_t)) = \mathbf{z}'_t \boldsymbol{\psi}_i$, with $\boldsymbol{\psi}_i \in \mathbb{R}^2$ for each $i \in \{1, 2, \dots, k-1\}$, thereby ensuring positive coefficient functions. We found this form to be flexible enough to capture the range of dependence trends considered in the study, though additional polynomial terms and/or coefficient functions could be added for more complex data structures.

4.4 Simulation study

We evaluate the properties of estimators proposed in Section 3 and compare these to the estimator derived in Mhalla et al. (2019), which we denote $\bar{\lambda}_{GAM}^*$. For the latter approach,

the thresholds used to define exceedances of the min-projection are set to be constant over the covariate space: this assumption is not required for $\bar{\lambda}_{QR}^*$ or $\bar{\lambda}_{BP}^*$.

To obtain ADF estimates using $\bar{\lambda}_{GAM}^*$, the same covariate set is used as for the quantile regression procedure, i.e., $\mathbf{z}_t = \{1, t, t^2, t^3\}$. This link function proposed in Mhalla et al. (2019) imposes the lower bound of $\lambda(w) = \max(w, 1 - w)$, but also imposes an upper bound of $\lambda(w) = 1$, meaning negative dependence cannot be captured. To relax this constraint, we instead consider the link function $h_w(x) = \log(x - \max(w, 1 - w))$, $x \in [\max(w, 1 - w), \infty)$, $w \in [0, 1]$ when estimating the ADFs for the negatively correlated Gaussian example. This ensures the lower bound is still satisfied for each example, while allowing all forms of extremal dependence to be captured. We also impose the boundary conditions discussed in Section 3.5 for $w = 0$ and $w = 1$. Furthermore, to ensure comparability, the final estimator is obtained as an average over 10 equally spaced quantiles in the interval $[0.9, 0.95]$. Such quantiles are used to define threshold exceedances of the min-projection variable prior to GAM fitting. We observe that imposing the upper bound $\lambda(w) = 1$ for $\bar{\lambda}_{GAM}^*$ in the majority of considered examples results in this estimator having a practical advantage over $\bar{\lambda}_{QR}^*$ and $\bar{\lambda}_{BP}^*$, since the latter estimators can exceed this upper bound.

To evaluate the performance of the estimators, estimates of the mean integrated squared error (MISE) were obtained using 250 samples from each copula. Given an estimator $\bar{\lambda}^*$, the MISE at time t is given by

$$\text{MISE}(\bar{\lambda}^*(\cdot | \mathbf{z}_t)) = \mathbb{E} \left(\int_0^1 [\bar{\lambda}^*(w | \mathbf{z}_t) - \lambda(w | \mathbf{Z}_t = \mathbf{z}_t)]^2 dw \right),$$

with smaller MISE values corresponding to estimators with lower bias and variance. Three different time points, $t = 1$, $t = n/2$ and $t = n$, were considered, corresponding to the start, middle and end of the simulated time frame, respectively.

Table 1 gives MISE values for each estimator and copula example at each time point. One can observe the lowest MISE values are always for $\bar{\lambda}_{BP}^*$ or $\bar{\lambda}_{GAM}^*$; this is likely due to

the reduced variance of these estimators compared to $\bar{\lambda}_{QR}^*$, owing to their semi-parametric forms. We also compared the integrated squared error (ISE) of median estimators, obtained pointwise over w for each method; in this case, the median estimator for $\bar{\lambda}_{QR}^*$ often gives the lowest ISE values. These additional results can be found in the Supplementary Material.

We observe that the MISE values for the negatively correlated Gaussian copula at the start of the interval ($t = 1$) are significantly larger than other MISE values. This is due to the fact that for strongly negatively dependent data structures, the value of the true ADF tends towards infinity as ρ approaches -1 for any ray $w \in (0, 1)$, which is difficult to capture in practice. However, we note that while significant bias appears to exist in ADF estimates, we are still able to obtain accurate return curve estimates, as discussed in Section 4.5.

Focusing on $t = 1, t = n/2$ and $t = n$, the MISE results for $\bar{\lambda}_{BP}^*$ and $\bar{\lambda}_{GAM}^*$ appear comparable; however, this is not the case if we consider the time frame as a whole. For this, we fix rays $w \in \{0.1, 0.3, 0.5\}$ and compute estimates of the ADF across 250 simulated examples. The median of the ADF estimates, alongside 0.025 and 0.975 quantiles, are calculated for each ray and time point $t \in \{1, \dots, n\}$ and these estimates are then plotted over time for fixed rays. The resulting plots for the inverted logistic copula are illustrated in Figure 3. As can be observed, the median estimates appear very close to the true ADF values for both our estimators proposed in Section 3. The uncertainty is lower for $\bar{\lambda}_{BP}^*$ compared to $\bar{\lambda}_{QR}^*$, owing to the former's semi-parametric form. Furthermore, both of our estimators appear to show lower bias on average compared to $\bar{\lambda}_{GAM}^*$, particularly for $w = 0.3$ and $w = 0.5$. Similar results are obtained for each of the copula examples, with the exception of the negatively correlated Gaussian copula: in this case, significant bias arises nearer the start of the time interval for each estimator, owing to the infinite upper bound for λ as $\rho \rightarrow -1$. The resulting plots can be found in the Supplementary Material. These results suggest higher bias for $\bar{\lambda}_{GAM}^*$ compared to the estimators proposed in Section

Table 1: MISE values for each estimator at start, middle and end of simulated time frame.

Smallest MISE values in each row are highlighted in bold.

Copula	Times	MISE - $\bar{\lambda}_{QR}^*$	MISE - $\bar{\lambda}_{BP}^*$	MISE - $\bar{\lambda}_{GAM}^*$
Gaussian (Positive Correlation)	Start	0.03375	0.01012	0.00497
Gaussian (Positive Correlation)	Middle	0.00356	0.0021	0.00229
Gaussian (Positive Correlation)	End	0.01978	0.00407	0.00143
Gaussian (Negative Correlation)	Start	32.24126	35.76231	30.10062
Gaussian (Negative Correlation)	Middle	0.08607	0.08646	0.06309
Gaussian (Negative Correlation)	End	0.02546	0.00849	0.00611
Inverted Logistic	Start	0.02075	0.00541	0.00315
Inverted Logistic	Middle	0.00209	0.00107	0.00627
Inverted Logistic	End	0.03539	0.00893	0.02744
Inverted Hüsler-Reiss	Start	0.05748	0.02017	0.03849
Inverted Hüsler-Reiss	Middle	0.00177	0.00065	0.00089
Inverted Hüsler-Reiss	End	0.01741	0.0057	0.00367
Inverted Asymmetric Logistic	Start	0.02771	0.00602	0.01863
Inverted Asymmetric Logistic	Middle	0.00279	0.00142	0.01995
Inverted Asymmetric Logistic	End	0.02956	0.00641	0.01406
Copula of model (4.1)	Start	0.0156	0.00621	0.00683
Copula of model (4.1)	Middle	0.00208	0.00088	0.01775
Copula of model (4.1)	End	0.04873	0.01486	0.00392

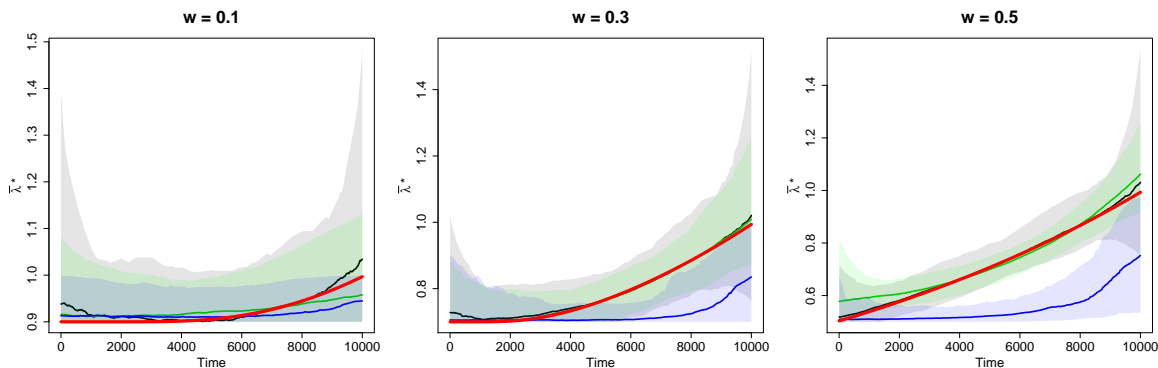


Figure 3: Plots of median and 95% confidence interval estimates over time at rays $w \in \{0.1, 0.3, 0.5\}$ for the inverted logistic copula. Red lines correspond to true ADF values, while the black, green and blue lines correspond to the median estimates for $\bar{\lambda}_{QR}^*$, $\bar{\lambda}_{BP}^*$ and $\bar{\lambda}_{GAM}^*$, respectively, with the coloured regions representing the estimated confidence intervals.

3.

Finally, we fix the time points $t = 1, t = n/2$ and $t = n$ and evaluate the variability in ADF estimates. Median curve estimates, alongside pointwise 95% confidence intervals, are obtained for each of the copula examples. Similar findings are reported for each of the estimators as have been discussed above. Plots of the estimated median curves and confidence regions for each estimator can be found in the Supplementary Material.

From these results, we conclude that the proposed estimators from Section 3 outperform the GAM-based estimator $\bar{\lambda}_{GAM}^*$ in a wide range of scenarios. This can be partly explained by the fact these estimators do not make the assumption of a constant threshold over time for the min-projection variable, leading to more realistic estimates. Moreover, we note that these results hold even though $\bar{\lambda}_{GAM}^*$ has the additional advantage of a link function which bounds the resulting ADF estimates for examples exhibiting positive extremal dependence. We therefore choose not to consider this GAM-based estimator further.

4.5 Return curve estimates

We now consider our ultimate goal of estimating return curves, $\text{RC}_{\mathbf{z}_t}(p)$, for extreme survival probabilities. Curve estimates $\overline{\text{RC}}_{\mathbf{z}_t}(p)$ at $p = 1/n$ under $\bar{\lambda}_{QR}^*$ and $\bar{\lambda}_{BP}^*$ were obtained for 250 simulated examples from each copula. To give an overall impression of the bias from each estimator, we fix a time point t and plot the median of the 250 estimates for $\overline{\text{RC}}_{\mathbf{z}_t}(p)$. Specifically, since each coordinate of $\overline{\text{RC}}_{\mathbf{z}_t}(p)$ is associated with a ray $w \in [0, 1]$, we take the median along each ray. Median curve estimates for the negatively correlated Gaussian example are given alongside the true return curves in Figure 4. As can be observed, the estimated curves in each case closely resemble the true return curves. This is even true at the start of the observation period, for which significant bias in ADF estimators was observed. Return curve estimates for each of the other simulated examples were similar in accuracy; these plots can be found in the Supplementary Material. Note that in each case, none of the theoretical properties for return curves derived in Murphy-Barltrop et al. (2021) have been applied.

5 UKCP18 case study

5.1 Properties of data

We denote the dataset introduced in Section 1 as $\{X_t, Y_t\}$ for $t \in \{1, \dots, n\}$, with X_t and Y_t corresponding to the temperature and dryness variables, respectively. In this case, we have $n = 9000$, corresponding to 100 years of summer projections from June 1981 to August 2080. We treat the time index t as a covariate for this data; while this does not correspond to any physical process, it can be used to capture the non-stationarity present in the data. For the marginal time series, empirical evidence indicates the presence of seasonal and long term trends within the main bodies of both variables. Further exploratory analysis

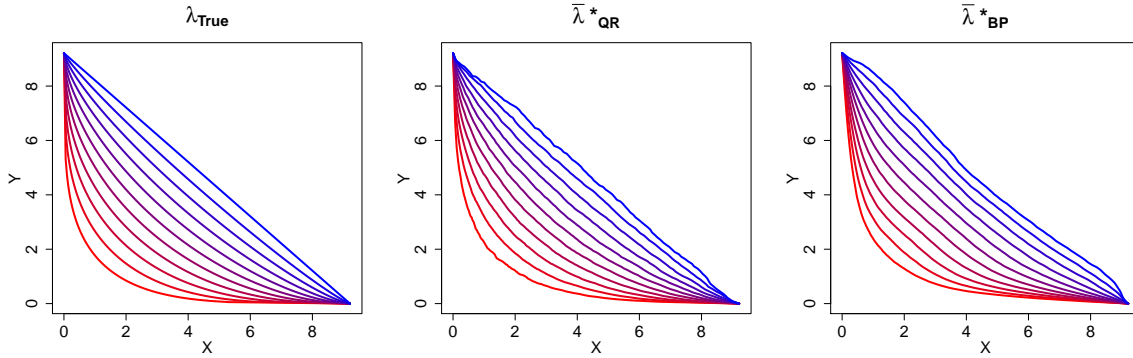


Figure 4: Plots of median return curve estimates over time with $p = 1/n$ for the Gaussian copula with negative correlation. Colour change illustrates extremal dependence trends over time, with red and blue correspond to start and end of time frame, respectively. True curves given in left panel, with estimated curves from the median estimators of $\bar{\lambda}_{QR}^*$ and $\bar{\lambda}_{BP}^*$ given in centre and right panels, respectively.

suggests the presence of non-stationary behaviour within dryness extremes and that non-stationarity is present within the extremal dependence structure, as evidenced by the trend in η in Figure 1. In this section, we attempt to account for all three forms of non-stationary trends and produce return curve estimates up to the end of the observation period.

5.2 Capturing marginal non-stationarity

To capture marginal non-stationarity, we extend the pre-processing technique described in equation (2.3), with the goal of removing any marginal trends from the data. Rather than specifying linear parametric forms for the covariate functions, as in Eastoe and Tawn (2009), we instead assume the residual process R_t is a sequence of standard normal variables and allow μ and σ to be general smooth functions of covariate vectors. These functions can be estimated using a GAM framework, allowing for flexible modelling of the marginal trends.

The time series in both cases appear to exhibit long term trends in location and scale,

along with seasonal behaviour within the former. Therefore, for the location function μ , and scale function σ , we take $\mathbf{z}_t = \{1, t, d_t\}$ and $\mathbf{z}_t = \{1, t\}$, respectively, where $d_t \in \{1, 2, \dots, 90\}$ denotes the day index of the process at time t . For example, d_t equals 1, 45, and 90 for June 1st, July 15th and August 30th, respectively. A thin plate regression spline is used for the covariate t , while for d_t , a cubic regression spline of dimension 90 (corresponding to the number of data points in each year) is used.

The fitting of the location and scale covariate functions is carried out using the R package `mgcv` (Wood, 2021), with a `gauss` family. Model optimisation is achieved via restricted maximum likelihood estimation, with smoothness penalties and knot quantities selected automatically using generalised cross validation. Further details for these modelling procedures can be found in Wood (2017). The resulting fitted trends are in good agreement with empirical estimates from the marginal time series: see the Supplementary Material for the corresponding plots. Moreover, the transformed series appear stationary, with no obvious long term or seasonal trends in either the location or scale.

With non-stationary trends in both marginal bodies accounted for, residual processes can be obtained through the transformations $R_{X_t} = [X_t - \mu_X(\mathbf{z}_t)]/\sigma_X(\mathbf{z}_t)$ and $R_{Y_t} = [Y_t - \mu_Y(\mathbf{z}_t)]/\sigma_Y(\mathbf{z}_t)$, where (μ_X, σ_X) and (μ_Y, σ_Y) denote the estimated covariate functions for X_t and Y_t , respectively. Assuming an accurate model fit, these processes should be approximately stationary within the body of the data. However, non-stationary trends are likely to remain in the tails since GAM fitting is driven by the body. Following Eastoe and Tawn (2009), we fit the non-stationary GPD described in equation (2.2) to capture any remaining trends. Significant linear and harmonic trends are shown to exist within the scale parameter of the residual process for dryness, while the shape parameter is assumed to be fixed over time. This assumption is common within the analysis of non-stationary univariate extremes (e.g. Eastoe and Tawn, 2009; Chavez-Demoulin and Davison, 2012), since the shape parameter is often seen as an intrinsic property of a physical process.

No significant trends were found for the scale parameter corresponding to the temperature variable. Let $\{(r_{X_t}, r_{Y_t}) : t = 1, \dots, n\}$ denote a data sample corresponding to the residuals vector (R_{X_t}, R_{Y_t}) . An estimate of the marginal distribution function $F_{R_{Y_t}}$ is given by

$$\hat{F}_{R_{Y_t}}(r \mid \mathbf{Z}_t = \mathbf{z}_t) = \begin{cases} 1 - (1 - q_Y)\{1 + \hat{\xi}_Y(r - u_Y)/\hat{\tau}_Y(\mathbf{z}_t)\}^{-1/\hat{\xi}_Y} & \text{for } r > u_Y, \\ \sum_{t=1}^n \mathbb{1}(r_{Y_t} \leq r)/(n+1) & \text{for } r \leq u_Y, \end{cases} \quad (5.1)$$

where $\mathbb{1}$ denotes an indicator function, u_Y is the empirical q_Y quantile of R_{Y_t} , and $(\hat{\tau}_Y(\mathbf{z}_t), \hat{\xi}_Y)$ are the MLEs of the GPD scale and shape parameters. The stationary GPD, denoted in equation (2.1), is used to estimate the upper tail of $F_{R_{X_t}}$.

Finally, the data is transformed to standard exponential margins via the probability integral transform. To assess the outcome of the pre-processing procedure, exponential rate parameters were estimated over time for both marginal processes. The resulting estimates remain approximately constant at one (the target value) throughout the observation period; an illustrative plot can be found in the Supplementary Material.

5.3 Model fitting

With the data transformed to standard exponential margins, we apply the methodology proposed in Section 3 for return curve estimation. The extremal dependence trend observed in Figure 1 appears to suggest the extremes of the process are becoming more positively dependent over the time frame; therefore, one may expect the ADF estimates to tend towards the lower bound as $t \rightarrow n$.

We set $\mathbf{z}_t := \{1, t\}$ for both the quantile regression procedure and estimation of Bernstein polynomial coefficients. This reduced covariate space was flexible enough to capture the observed extremal dependence trend within the data. Moreover, the same set of quantile pairs $\{q_{1,j}, q_{2,j}\}_{j=1}^m$ was considered as defined in Section 4.3. Two sets of ADF estimates are obtained over the observation period corresponding to $\bar{\lambda}_{QR}^*$ and $\bar{\lambda}_{BP}^*$; these are plotted in

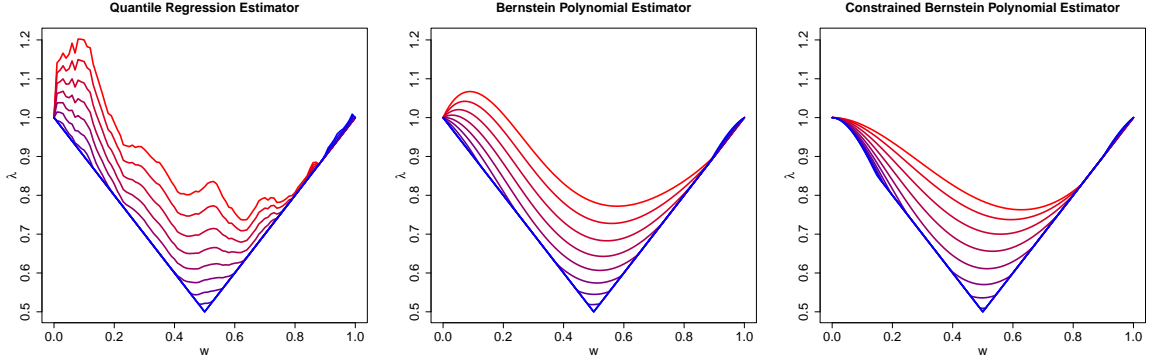


Figure 5: Left, centre and right: ADF estimates over time for $\bar{\lambda}_{QR}^*$, $\bar{\lambda}_{BP}^*$ and constrained $\bar{\lambda}_{BP}^*$, respectively. Curves change from red to blue over the observation period.

the left and centre panels of Figure 5, respectively. The selected values of t for the plotted curves correspond to July 15th for an increasing subset of years between 1981-2080.

However, we note that for both estimators, we obtain ADFs which exceed one at several rays; this is unexpected, since exploratory analysis of the data appears to suggest the presence of positive dependence over the entire time frame. While $\lambda(w) < 1$ or $\lambda(w) > 1$ for all $w \in (0, 1)$ indicate positive and negative extremal dependence, respectively, intermediate scenarios where $\lambda(w) > 1$ for some rays and $\lambda(w) < 1$ for others are theoretically possible. Having investigated this aspect, the evidence that $\lambda(w) > 1$ for small w is not strong, and so we seek to implement an estimator which is bounded above by one. We therefore re-apply the Bernstein polynomial estimator, this time constraining the coefficient functions to be in the interval $[0, 1]$ via a logit link function, i.e., $\text{logit}(\beta_i(\mathbf{z}_t)) = \mathbf{z}_t' \boldsymbol{\psi}_i$, $\boldsymbol{\psi}_i \in \mathbb{R}^2$, $i \in \{1, 2, \dots, k - 1\}$. The resulting ADF estimates are illustrated in the right panel of Figure 5. The estimated trends are again in good agreement with what is observed in the data.

To evaluate uncertainty in estimates, we propose a block bootstrapping procedure. First, the data on exponential margins is split into segments of size 450, corresponding to five years of observations. The extremal dependence structure within such segments is then

assumed to be approximately stationary. Within each segment, data is then resampled in blocks of size 15 with replacement to account for temporal dependence. These blocks are combined to form a resampled segment, then each of the segments are merged in order to obtain a new dataset. This process is repeated 250 times to generate sets of ADF estimates while accounting for complex structures in the data. The median of the estimated ADFs for $t = n/2$, alongside 95% pointwise confidence intervals, are illustrated in the left panel of Figure 6 for the Bernstein polynomial estimator with constrained coefficients.

Finally, to assess the quality of the ADF estimates, we have compared the model estimates of η over time, obtained via the constrained version of $\bar{\lambda}_{BP}^*$, to the empirical estimates introduced in Section 1. For each rolling window, we have taken the average η estimate from the fitted model. As illustrated in the centre panel of Figure 6, the model estimates appear similar over time, suggesting we have accurately captured the extremal dependence trend at this ray.

5.4 Return curve estimates

We use our estimated ADFs to estimate return curves $\overline{RC}_{z_t}(p)$ up to the year 2080. This is done in two steps: first, we apply the method introduced in Section 3.6 to obtain return curve estimates on standard exponential margins. These curves are then transformed back to the original scale by applying the the inverse of the empirical distribution given in equation (2.2), followed by the inverses of the transformations used to obtain the variables R_{X_t} and R_{Y_t} . The right panel of Figure 6 illustrates the return curve estimates for the vector (X_t, Y_t) , obtained using the constrained version of $\bar{\lambda}_{BP}^*$, with $p = 1/n$; this corresponds to an extreme probability, relative to the size of dataset. The selected values of t for the plotted curves again correspond to July 15th for an increasing subset of years between 1981-2080. All of the theoretical properties for return curves introduced in Murphy-Barltrop et al. (2021) have been imposed to ensure the resulting estimates are both theoretically possible

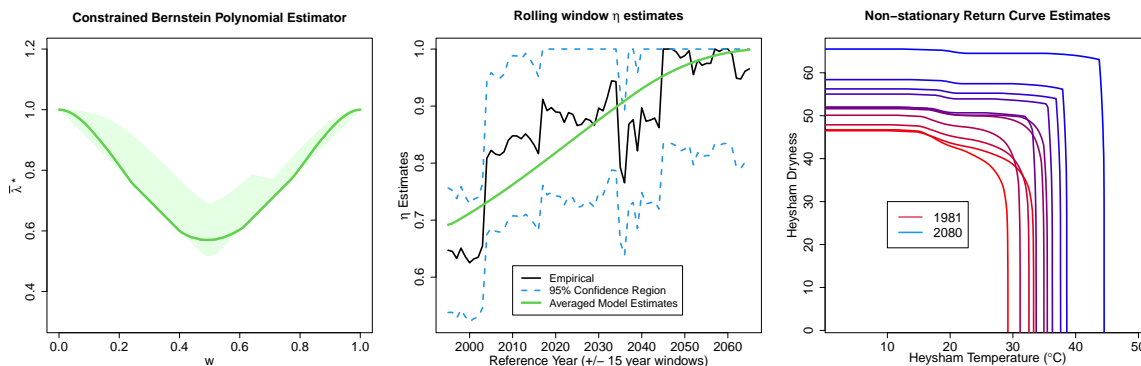


Figure 6: Left: median ADF estimate for $t = n/2$ obtained through bootstrapping procedure, with coloured region representing uncertainty bounds. Centre: Comparison of averaged model η estimates for rolling windows to empirical estimates, with black, green and dotted blue lines corresponding to empirical, model, and 95% confidence interval estimates respectively. Right: Return curve estimates on original margins with $p = 1/n$ at July 15th over the observation period. Time is illustrated using a colour transition, with red and blue curves correspond to start and end of time frame, respectively.

and realistic.

From these curve estimates, two conclusions are evident. Firstly, clear marginal trends can be observed for both time series. For example, the temperature values at the point where the curves intersect the x -axis, which equate to $(1 - p)$ -th non-stationary quantile estimates, increase by over 10°C through the observation period. Moreover, a dependence trend is evidenced by the changing shape in return curve estimates over time, with the curves becoming increasingly ‘square’ shaped from 1981-2080. This suggests that joint extremes of temperature and dryness are becoming more likely to occur over the observation period.

6 Discussion

We have proposed a novel method for capturing non-stationary extremal dependence structures under asymptotic independence. Our method has been successfully applied to heavily non-stationary data from the UKCP18, allowing us to obtain return curve estimates up to the year 2080 and thereby illustrating how this framework could help improve practical risk management under future climate scenarios.

We have investigated the properties of our estimators via simulation and have observed them generally perform well in terms of bias. While it would be desirable also to have theoretical results on bias of the estimators, this is very challenging in practice and is likely to require assumptions that are too strict to make the results worthwhile. Potentially a more promising line of future work would be the development of diagnostic plots for non-stationary ADF and return curve estimates. Our diagnostic procedures were limited to comparison of rolling window η estimates against those derived from the ADF. In general, diagnostic plots for return curves, such as those introduced in Murphy-Barltrop et al. (2021), require stationarity assumptions.

For the sake of simplicity, we have restricted attention to the bivariate setting. However, it is worth noting that all methods could in principle be extended to the general multivariate setting. This scenario results in additional modelling complexities, since different extremal dependence regimes can exist within subvectors of a multivariate random vector. Moreover, applications of multivariate extremal risk measures are limited, owing in part to the fact visualisation and interpretation becomes more challenging in this setting.

As noted in Section 3.5, imposing the lower bound on the estimates of the ADF was shown to improve the estimation procedure. This was an ad-hoc post-processing step, with many of the obtained ADF estimates below the bound. Future work could explore how this lower bound could be incorporated into the theoretical quantile regression frame-

work, and whether this would further improve the quality of ADF estimates. We note that when asymptotic dependence is present, $\lambda(w \mid \mathbf{z}_t) = \max(w, 1 - w)$ will cease to depend on \mathbf{z}_t . However, return curve estimates $\overline{\text{RC}}_{\mathbf{z}_t}(p)$ are also affected by the sequences $\{u_{w,t}\}$ as described in Section 3.6, so will still capture non-stationarity. Nonetheless, if asymptotic dependence is clearly present at all time points, other techniques for estimating non-stationarity may be preferable.

We recognise that the method proposed for evaluating and representing uncertainty in Section 5 relies on strong assumptions and is an approximation of the true uncertainty. Theoretical derivation of uncertainty intervals for either of the estimators proposed in Section 3 is not possible, meaning any evaluation of uncertainty must be non-parametric. Uncertainty quantification is a general problem when modelling non-stationary processes, since the underlying datasets cannot be resampled using a straightforward bootstrapping procedure.

Finally, we note that the data within the climate projections exhibits non-negligible temporal dependence. This feature decreases the amount of information available, and we found that the ADF estimation procedures detailed in Section 3 performed worse when this feature was present. However, for ease of implementation, we have assumed independence in both marginal distributions. Techniques for incorporating temporal dependence with quantile regression (Koenker et al., 2017) could be incorporated into our methodology in future work.

Acknowledgements

This paper is based on work completed while Callum Murphy-Barltrop was part of the EPSRC funded STOR-i centre for doctoral training (EP/L015692/1).

SUPPLEMENTARY MATERIAL

Supplementary Material for “Modelling non-stationarity in asymptotically

independent extremes” We provide additional figures relevant to the UKCP18 dataset;

in particular, plots related to the varying extremal dependence across seasons and modelling of marginal non-stationarity. We also include additional supporting results for the simulation study described in Section 4, which further illustrate ADF and return curve estimates across the considered examples.

Case Study Program We provide an *R* program to generate the case study plots discussed in Section 5. These plot relate to estimation of the marginal distributions and of non-stationary ADFs and return curves via the constrained version of $\bar{\lambda}_{BP}^*$.

References

- Balkema, A. A. and de Haan, L. (1974). Residual Life Time at Great Age. *The Annals of Probability*, 2(5).
- Cade, B. S. and Noon, B. R. (2003). A Gentle Introduction to Quantile Regression for Ecologists. *Frontiers in Ecology and the Environment*, 1(8):412.
- Castro-Camilo, D., de Carvalho, M., and Wadsworth, J. (2018). Time-varying extreme value dependence with application to leading european stock markets. *Annals of Applied Statistics*, 12(1):283–309.
- Chavez-Demoulin, V. and Davison, A. C. (2005). Generalized additive modelling of sample extremes. *Journal of the Royal Statistical Society: Series C (Applied Statistics)*, 54(1):207–222.
- Chavez-Demoulin, V. and Davison, A. C. (2012). MODELLING TIME SERIES EXTREMES. Technical Report 1.

- Chernozhukov, V. (2004). Inference for Extremal Conditional Quantile Models.
- Chernozhukov, V. and Fernández-Val, I. (2011). Inference for extremal conditional quantile models, with an application to market and birthweight risks. *Review of Economic Studies*, 78(2):559–589.
- Chernozhukov, V., Fernández-Val, I., and Kaji, T. (2017). Extremal quantile regression. *Handbook of Quantile Regression*, (2005):333–362.
- Coles, S. (2001). *An Introduction to Statistical Modeling of Extreme Values*. Springer Series in Statistics. Springer London, London.
- Coles, S., Heffernan, J., and Tawn, J. (1999). Dependence measures for multivariate extremes. *Extremes*, 2(4):339–365.
- Coles, S. G. and Tawn, J. A. (1991). Modelling Extreme Multivariate Events. *Journal of the Royal Statistical Society. Series B: Statistical Methodology*, 53(2):377–392.
- Davison, A. C. and Smith, R. L. (1990). Models for Exceedances Over High Thresholds. *Journal of the Royal Statistical Society: Series B (Methodological)*, 52(3):393–425.
- de Carvalho, M. and Davison, A. C. (2014). Spectral density ratio models for multivariate extremes. *Journal of the American Statistical Association*, 109(506):764–776.
- Eastoe, E. F. and Tawn, J. A. (2009). Modelling non-stationary extremes with application to surface level ozone. *Journal of the Royal Statistical Society. Series C: Applied Statistics*, 58(1):25–45.
- Frahm, G. (2006). On the extremal dependence coefficient of multivariate distributions. *Statistics and Probability Letters*, 76(14):1470–1481.
- Gouldby, B., Wyncoll, D., Panzeri, M., Franklin, M., Hunt, T., Hames, D., Tozer, N., Hawkes, P., Dornbusch, U., and Pullen, T. (2017). Multivariate extreme value modelling

- of sea conditions around the coast of England. *Proceedings of the Institution of Civil Engineers: Maritime Engineering*, 170(1):3–20.
- Guerrero, M. B., Huser, R., and Ombao, H. (2021). Conex-Connect: Learning Patterns in Extremal Brain Connectivity From Multi-Channel EEG Data.
- Guillotte, S. and Perron, F. (2016). Polynomial Pickands functions. *Bernoulli*, 22(1):213–241.
- Heffernan, J. E. and Tawn, J. A. (2004). A conditional approach for multivariate extreme values. *Journal of the Royal Statistical Society. Series B: Statistical Methodology*, 66(3):497–546.
- Hill, B. M. (1975). A Simple General Approach to Inference About the Tail of a Distribution. *The Annals of Statistics*, 3(5):1163–1174.
- Huser, R. and Wadsworth, J. L. (2019). Modeling Spatial Processes with Unknown Extremal Dependence Class. *Journal of the American Statistical Association*, 114(525):434–444.
- Jonathan, P., Ewans, K., and Flynn, J. (2014a). On the estimation of ocean engineering design contours. *Journal of Offshore Mechanics and Arctic Engineering*, 136(4):1–8.
- Jonathan, P., Ewans, K., and Randell, D. (2014b). Non-stationary conditional extremes of northern North Sea storm characteristics. *Environmetrics*, 25(3):172–188.
- Keef, C., Papastathopoulos, I., and Tawn, J. A. (2013). Estimation of the conditional distribution of a multivariate variable given that one of its components is large: Additional constraints for the Heffernan and Tawn model. *Journal of Multivariate Analysis*, 115:396–404.

- Knochenhauer, M. and Louko, P. (2004). Guidance for External Events Analysis. In *Probabilistic Safety Assessment and Management*, pages 1498–1503. Springer, London.
- Koenker, R., Chernozhukov, V., He, X., and Peng, L. (2017). *Handbook of Quantile Regression*. Chapman and Hall/CRC.
- Krock, M., Bessac, J., Stein, M. L., and Monahan, A. H. (2021). Nonstationary seasonal model for daily mean temperature distribution bridging bulk and tails. pages 1–19.
- Kyselý, J., Pícek, J., and Beranová, R. (2010). Estimating extremes in climate change simulations using the peaks-over-threshold method with a non-stationary threshold. *Global and Planetary Change*, 72(1-2):55–68.
- Ledford, A. W. and Tawn, J. A. (1996). Statistics for near independence in multivariate extreme values. *Biometrika*, 83(1):169–187.
- Ledford, A. W. and Tawn, J. A. (1997). Modelling dependence within joint tail regions. *Journal of the Royal Statistical Society. Series B: Statistical Methodology*, 59(2):475–499.
- Manuel, L., Nguyen, P. T., Canning, J., Coe, R. G., Eckert-Gallup, A. C., and Martin, N. (2018). Alternative approaches to develop environmental contours from metocean data. *Journal of Ocean Engineering and Marine Energy*, 4(4):293–310.
- Marcon, G., Padoan, S. A., and Antoniano-Villalobos, I. (2016). Bayesian inference for the extremal dependence. *Electronic Journal of Statistics*, 10(2):3310–3337.
- Marcon, G., Padoan, S. A., Naveau, P., Muliere, P., and Segers, J. (2017). Multivariate nonparametric estimation of the Pickands dependence function using Bernstein polynomials. *Journal of Statistical Planning and Inference*, 183:1–17.
- Mentaschi, L., Vousdoukas, M., Voukouvalas, E., Sartini, L., Feyen, L., Besio, G., and Alfiéri, L. (2016). The transformed-stationary approach: A generic and simplified method-

- ology for non-stationary extreme value analysis. *Hydrology and Earth System Sciences*, 20(9):3527–3547.
- Mhalla, L., de Carvalho, M., and Chavez-Demoulin, V. (2019a). Regression-type models for extremal dependence. *Scandinavian Journal of Statistics*, 46(4):1141–1167.
- Mhalla, L., Opitz, T., and Chavez-Demoulin, V. (2019b). Exceedance-based nonlinear regression of tail dependence. *Extremes*, 22(3):523–552.
- Murphy-Bartrop, C. J. R., Wadsworth, J. L., and Eastoe, E. F. (2021). On the Estimation of Bivariate Return Curves for Extreme Values.
- Nogaj, M., Parey, S., and Dacunha-Castelle, D. (2007). Non-stationary extreme models and a climatic application. *Nonlinear Processes in Geophysics*, 14(3):305–316.
- Nolde, N. and Wadsworth, J. (2021). Linking representations for multivariate extremes via a limit set. *Advances in Applied Probability (to appear)*.
- Northrop, P. J. and Jonathan, P. (2011). Threshold modelling of spatially dependent non-stationary extremes with application to hurricane-induced wave heights. *Environmetrics*, 22(7):799–809.
- Office for Nuclear Regulation (2018). NS-TAST-GD-013 Revision 8. Technical report, Department for Work and Pensions.
- Pauli, F. and Coles, S. (2002). Models and inference for uncertainty in extremal dependence. *Biometrika*, 89(1):183–196.
- Pickands, J. (1975). Statistical Inference Using Extreme Order Statistics. *The Annals of Statistics*, 3(1):119–131.
- Resnick, S. I. (1987). *Extreme Values, Regular Variation and Point Processes*. Springer Series in Operations Research and Financial Engineering. Springer New York, New York.

- Ross, E., Astrup, O. C., Bitner-Gregersen, E., Bunn, N., Feld, G., Gouldby, B., Huseby, A., Liu, Y., Randell, D., Vanem, E., and Jonathan, P. (2020). On environmental contours for marine and coastal design. *Ocean Engineering*, 195:106194.
- Serinaldi, F. (2015). Dismissing return periods! *Stochastic Environmental Research and Risk Assessment*, 29(4):1179–1189.
- Sigauke, C. and Bere, A. (2017). Modelling non-stationary time series using a peaks over threshold distribution with time varying covariates and threshold: An application to peak electricity demand. *Energy*, 119:152–166.
- Stein, M. L. (2021). A parametric model for distributions with flexible behavior in both tails. *Environmetrics*, 32(2):e2658.
- Tawn, J. A. (1988). Bivariate extreme value theory: Models and estimation. *Biometrika*, 75(3):397–415.
- UK Met Office (2018). UKCP18 Guidance: Representative Concentration Pathways. pages 18–20.
- Velthoen, J., Dombry, C., Cai, J.-J., and Engelke, S. (2021). Gradient boosting for extreme quantile regression.
- Wadsworth, J. L. and Tawn, J. A. (2013). A new representation for multivariate tail probabilities. *Bernoulli*, 19(5 B):2689–2714.
- Wadsworth, J. L., Tawn, J. A., Davison, A. C., and Elton, D. M. (2017). Modelling across extremal dependence classes. *Journal of the Royal Statistical Society. Series B: Statistical Methodology*, 79(1):149–175.
- Wei, Y., Pere, A., Koenker, R., and He, X. (2006). Quantile regression methods for reference growth charts. *Statistics in Medicine*, 25(8):1369–1382.

Wood, S. (2021). Mixed GAM Computation Vehicle with Automatic Smoothness Estimation. *R Package*.

Wood, S. N. (2017). *Generalized Additive Models*. Chapman and Hall/CRC.

Youngman, B. (2020). evgam: Generalised Additive Extreme Value Models. *R Package*.

Youngman, B. D. (2019). Generalized Additive Models for Exceedances of High Thresholds With an Application to Return Level Estimation for U.S. Wind Gusts. *Journal of the American Statistical Association*, 114(528):1865–1879.

Supplementary Material for “Modelling non-stationarity in asymptotically independent extremes”

C. J. R. Murphy-Barltrop^{1*} and J. L. Wadsworth²

¹STOR-i Centre for Doctoral Training, Lancaster University LA1 4YR, United Kingdom

²Department of Mathematics and Statistics, Lancaster University LA1 4YF, United Kingdom

*Correspondence to: c.barltrop@lancaster.ac.uk

March 21, 2022

Keywords: Extremal Dependence, Non-stationary Processes, Multivariate Extremes

1 Varying extremal dependence structures across seasons for UKCP18 dataset

Trends in the extremal dependence structure for the UKCP18 projections were considered across each of the meteorological seasons independently. For a given season, the corresponding subset of data was transformed to exponential margins using the same techniques as described in the case study of the main text (Section 5). The coefficient η was then estimated across ± 15 year rolling windows over the observation period; the resulting plots for Autumn, Winter and Spring are given in the left, centre and right panels of Figure 1. These plots illustrate significantly different behaviour across these seasons, justifying our choice to just consider summer data within the case study. Moreover, summer is likely to correspond to the highest temperature and dryness values, hence it makes most sense to consider joint extremal behaviour for this season.

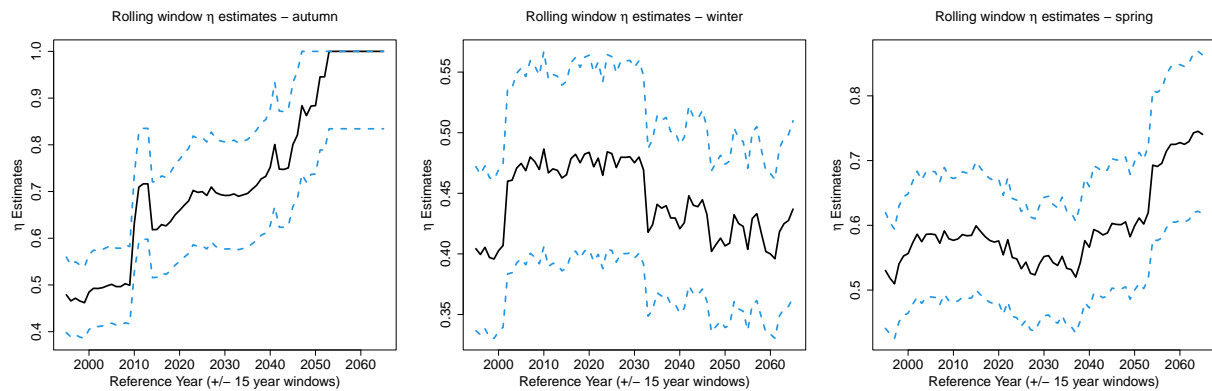


Figure 1: Trends in η parameter estimates (solid black lines) over ± 15 year rolling windows for autumn, winter and spring, alongside 95% pointwise confidence intervals (dotted blue lines).

2 Additional simulation study results

2.1 ISE values computed using median estimators.

Using 250 samples from each copula, median ADF estimators were computed pointwise over the set $\mathcal{W} = \{0, 0.01, 0.02, \dots, 0.99, 1\}$ for three different time points: $t = 1, t = n/2$ and $t = n$, corresponding to the start, middle and end of the simulated time frame, respectively. The integrated squared error (ISE) of the median estimators is used to compare performance across $\bar{\lambda}_{QR}^*$, $\bar{\lambda}_{BP}^*$ and $\bar{\lambda}_{GAM}^*$. Although these median estimators are not computable in a given application, understanding their properties gives an insight into the bias of the estimators. Letting $\text{med}_t \bar{\lambda}^*$ denote a median estimator at time t , the ISE is given by

$$\text{ISE}(\text{med}_t \bar{\lambda}^*(\cdot | \mathbf{z}_t)) = \int_0^1 [\text{med}_t \bar{\lambda}^*(w | \mathbf{z}_t) - \lambda(w | \mathbf{Z}_t = \mathbf{z}_t)]^2 dw,$$

with smaller ISE values corresponding to an estimator with lower bias. Table 1 gives the ISE values for each median estimator and copula example at each of the three time points. As can be observed, the ISE values are very similar for both $\bar{\lambda}_{QR}^*$ and $\bar{\lambda}_{BP}^*$, indicating similar bias for these estimators. Moreover, $\bar{\lambda}_{QR}^*$ often results in the lowest ISE values compared to the other two estimators.

2.2 Non-stationary ADF estimates over time

Figures 2 - 6 illustrate median estimates, alongside 0.025 and 0.975 quantile estimates, of the ADF at fixed rays over time for each copula example, excluding the inverted logistic copula which has already been considered in the main text. In each case, the rays $w = 0.1$, $w = 0.3$ and $w = 0.5$ have been considered and the black, green and blue lines correspond to the median estimates for $\bar{\lambda}_{QR}^*$, $\bar{\lambda}_{BP}^*$ and $\bar{\lambda}_{GAM}^*$, respectively, with the coloured regions representing the area between the pointwise 0.025 and 0.975 quantiles. For the inverted asymmetric logistic copula, two additional rays ($w = 0.7$ and $w = 0.9$) have been considered

Table 1: ISE values for median estimators at start, middle and end of simulated time frame.

Smallest ISE values in each row are highlighted in bold.

Copula	Times	ISE - $\bar{\lambda}_{QR}^*$	ISE - $\bar{\lambda}_{BP}^*$	ISE - $\bar{\lambda}_{GAM}^*$
Gaussian (Positive Correlation)	Start	0.00084	0.00138	0.00167
Gaussian (Positive Correlation)	Middle	0.00115	0.00110	0.00103
Gaussian (Positive Correlation)	End	0.00010	0.00035	0.00016
Gaussian (Negative Correlation)	Start	33.12202	36.09158	31.43350
Gaussian (Negative Correlation)	Middle	0.08161	0.08196	0.05865
Gaussian (Negative Correlation)	End	0.00040	0.00116	0.00025
Inverted Logistic	Start	0.00086	0.00041	0.00007
Inverted Logistic	Middle	0.00001	0.00009	0.00654
Inverted Logistic	End	0.00144	0.00145	0.01910
Inverted Hüsler-Reiss	Start	0.00582	0.00142	0.03454
Inverted Hüsler-Reiss	Middle	0.00001	0.00006	0.00037
Inverted Hüsler-Reiss	End	0.00026	0.00097	0.00019
Inverted Asymmetric Logistic	Start	0.00123	0.00033	0.01837
Inverted Asymmetric Logistic	Middle	0.00002	0.00002	0.01942
Inverted Asymmetric Logistic	End	0.00073	0.00038	0.00965
Copula of model (12)	Start	0.00084	0.00069	0.00405
Copula of model (12)	Middle	0.00004	0.00013	0.01519
Copula of model (12)	End	0.00888	0.00596	0.00381

to account for the asymmetry within this example.

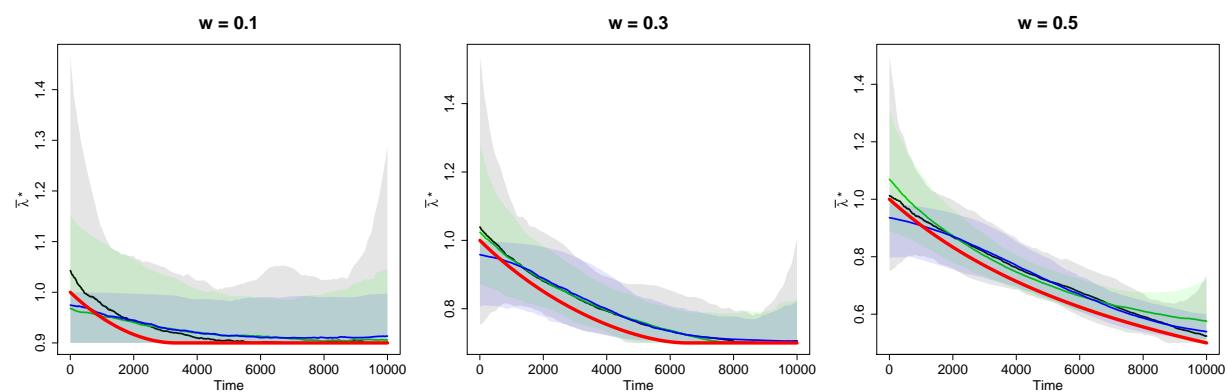


Figure 2: Non-stationary ADF estimates over time for the Gaussian copula with positive correlation.

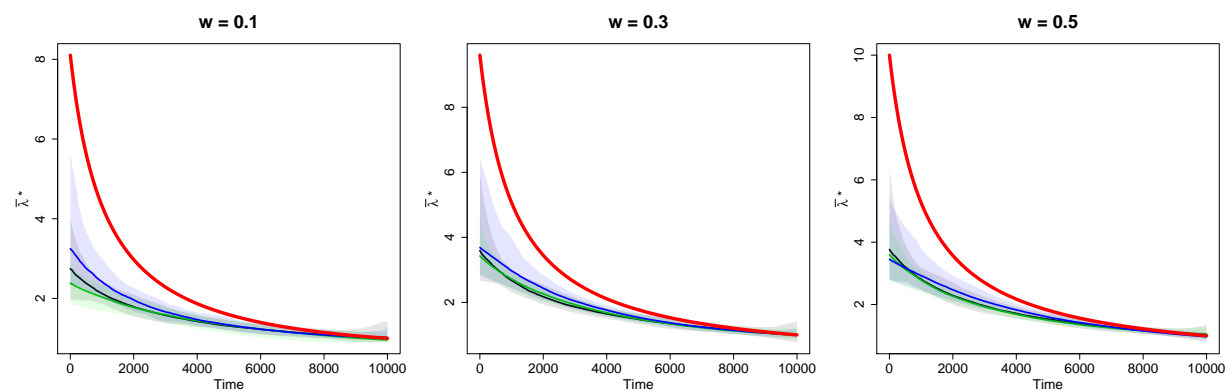


Figure 3: Non-stationary ADF estimates over time for the Gaussian copula with negative correlation.

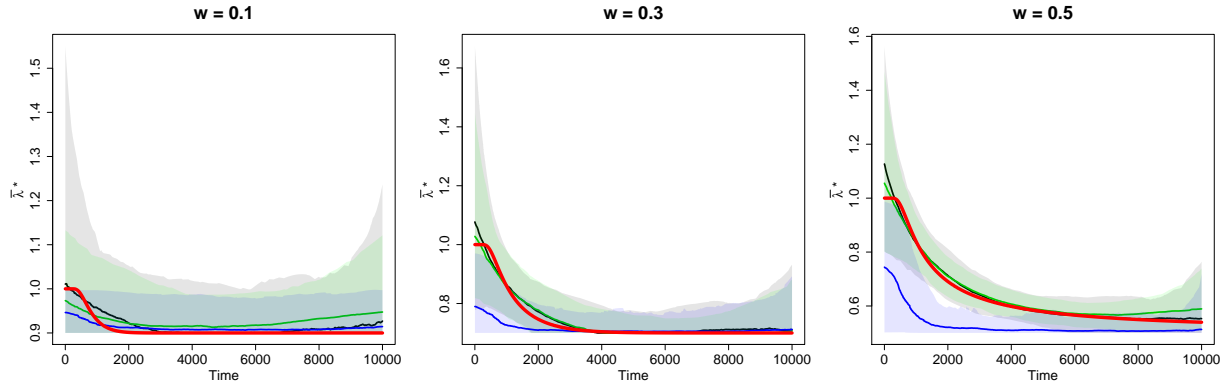


Figure 4: Non-stationary ADF estimates over time for the inverted Hüsler-Reiss copula.

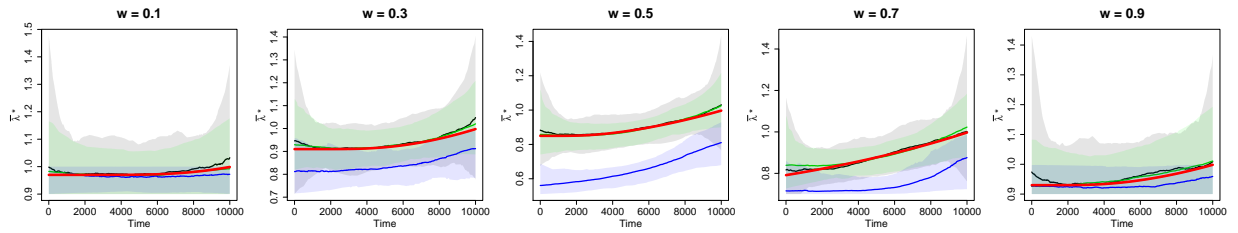


Figure 5: Non-stationary ADF estimates over time for the inverted asymmetric logistic copula.

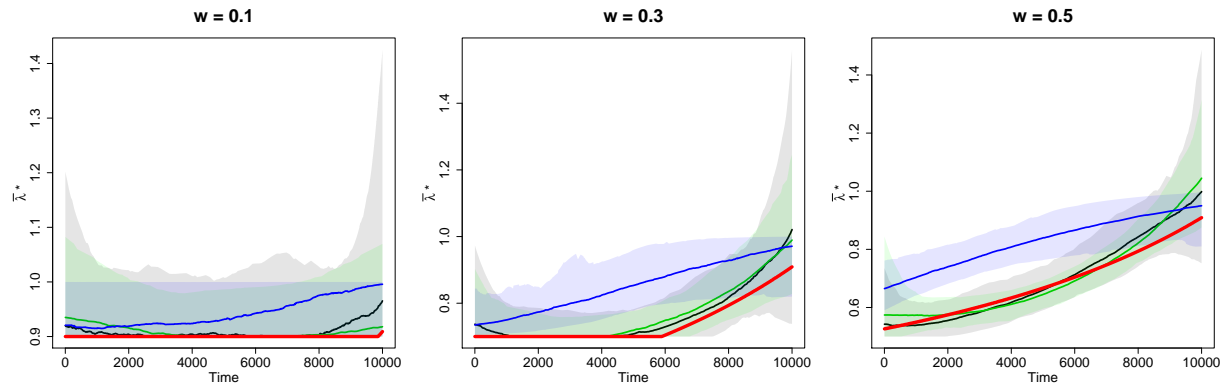


Figure 6: Non-stationary ADF estimates over time for the copula of model (12)

2.3 Non-stationary ADF estimates at fixed time points

Figures 7 - 12 illustrate median estimates, alongside 0.025 and 0.975 quantile estimates, of the ADF at three fixed time points ($t = 1$, $t = n/2$ and $t = n$) over all rays $w \in [0, 1]$ for each copula example. In each case, the red lines represent the true ADF functions, while the black, green and blue lines correspond to the median estimates for $\bar{\lambda}_{QR}^*$, $\bar{\lambda}_{BP}^*$ and $\bar{\lambda}_{GAM}^*$, respectively, with the coloured regions representing the area between the pointwise 0.025 and 0.975 quantiles.

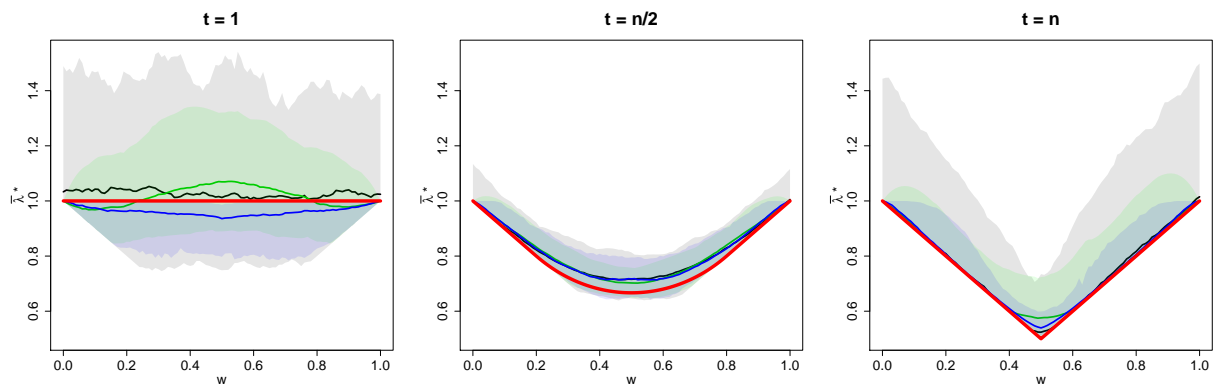


Figure 7: Non-stationary ADF estimates at three fixed time points for the Gaussian copula with positive correlation.

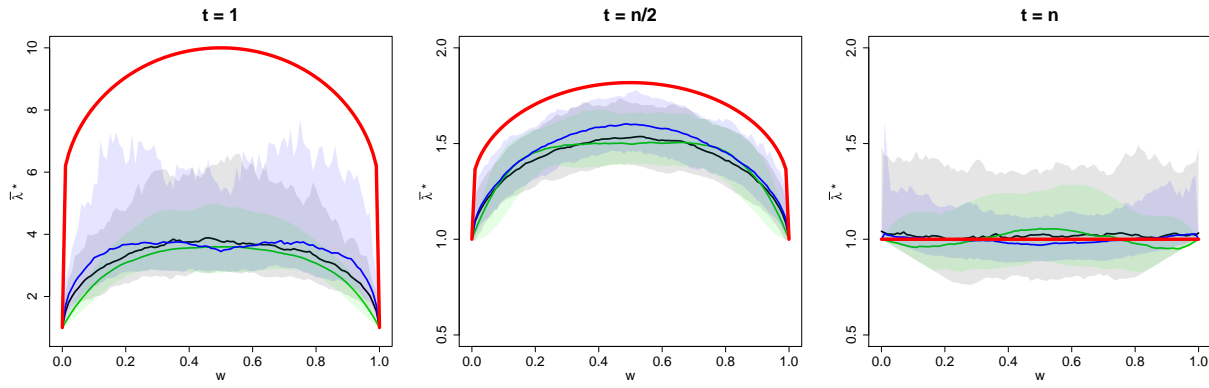


Figure 8: Non-stationary ADF estimates at three fixed time points for the Gaussian copula with negative correlation.

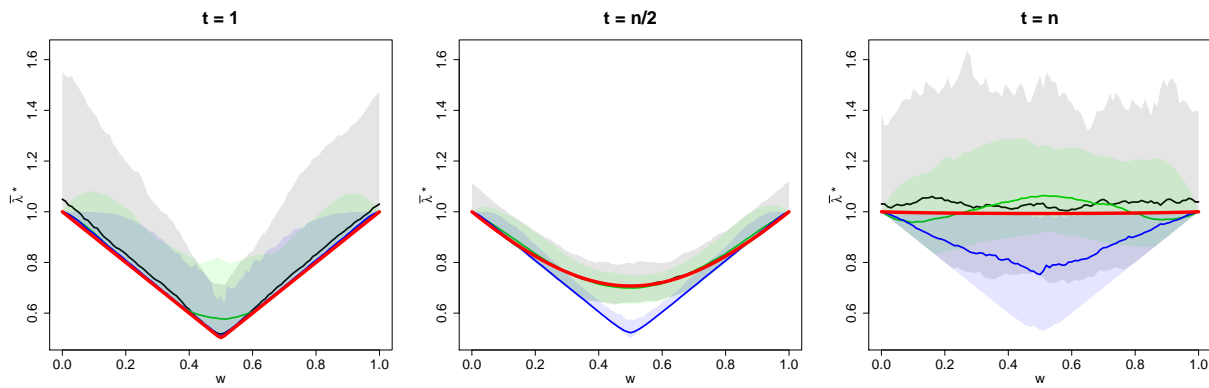


Figure 9: Non-stationary ADF estimates at three fixed time points for the inverted logistic copula.

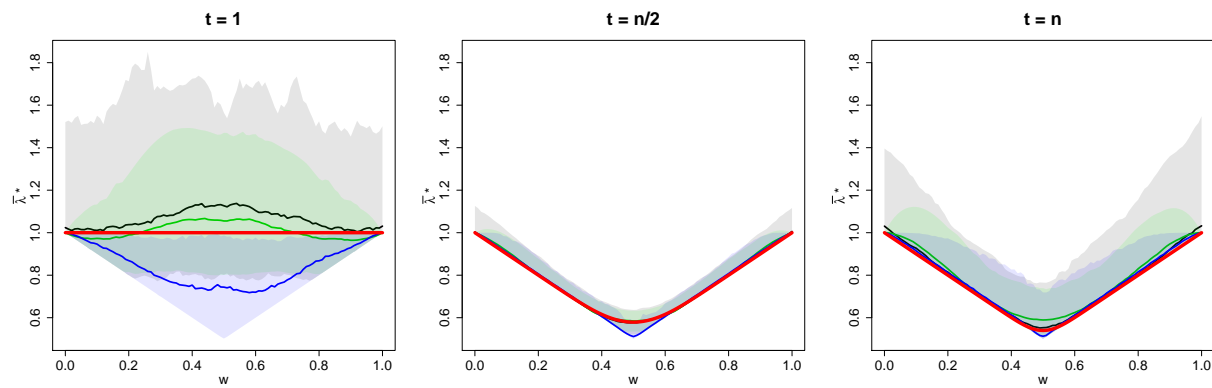


Figure 10: Non-stationary ADF estimates at three fixed time points for the inverted Hüsler-Reiss copula.

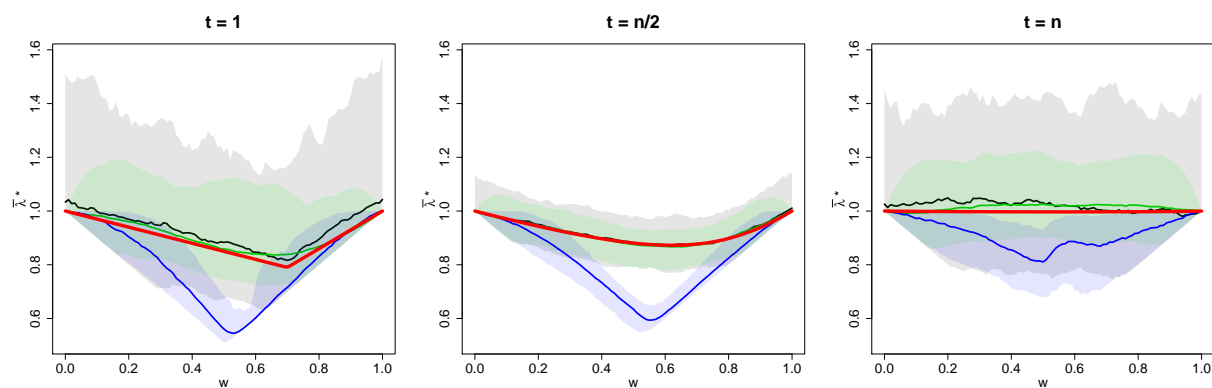


Figure 11: Non-stationary ADF estimates at three fixed time points for the inverted asymmetric logistic copula.

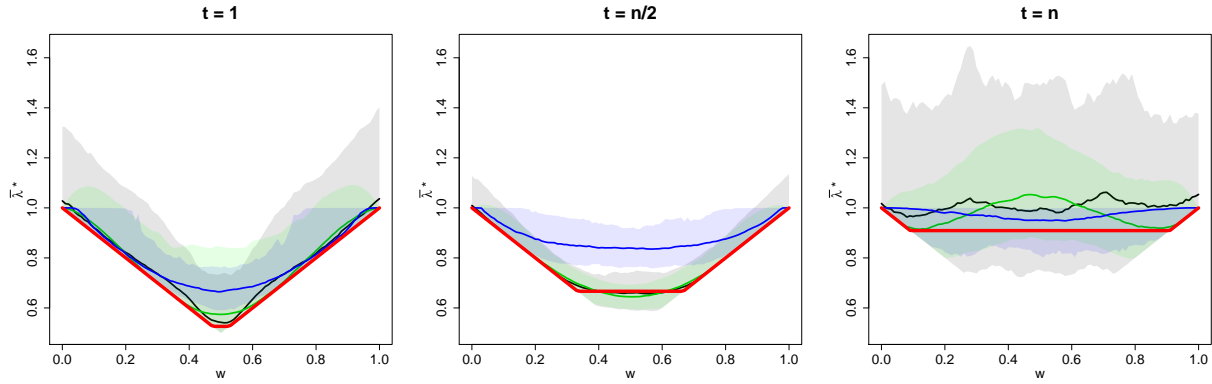


Figure 12: Non-stationary ADF estimates at three fixed time points for the copula of model (12).

2.4 Non-stationary return curve estimates

Figures 13 - 17 illustrate median estimates of $RC_{z_t}(p)$ at $p = 1/n$ obtained under $\bar{\lambda}_{QR}^*$ and $\bar{\lambda}_{BP}^*$ for each of the copula examples, excluding the Gaussian copula with negative correlation which has already been considered in the main text. In each case, the true return curves are given in the left panels, while the curves corresponding to $\bar{\lambda}_{QR}^*$ and $\bar{\lambda}_{BP}^*$ are given in the centre and right panels, respectively. Time is illustrated using a smooth curve colour change, with red and blue curves corresponding to the start and end of the time frame, respectively. We observe that the quality of the median curve estimates appear to be worse near both the start and end of the time frame. This is likely due to the larger degree of variability that arises at such time points, as exhibited in Figures 2 - 6.

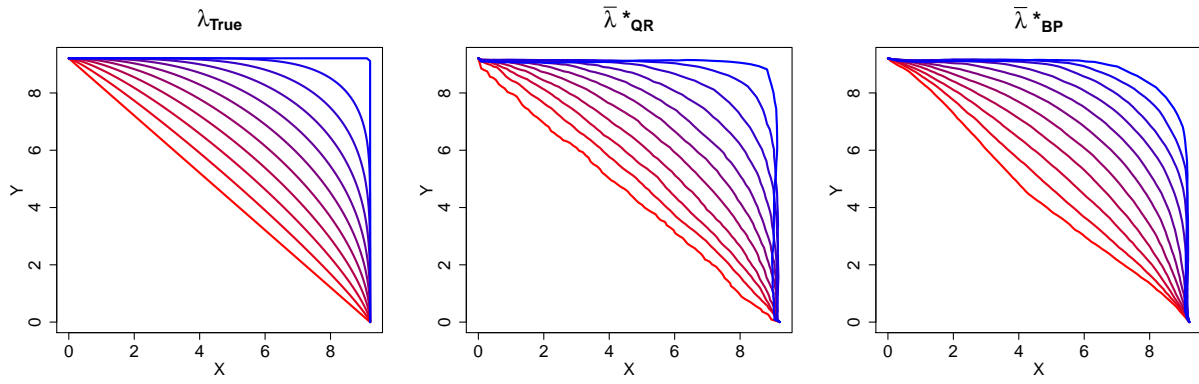


Figure 13: Non-stationary return curve estimates over time for the Gaussian copula with positive correlation.

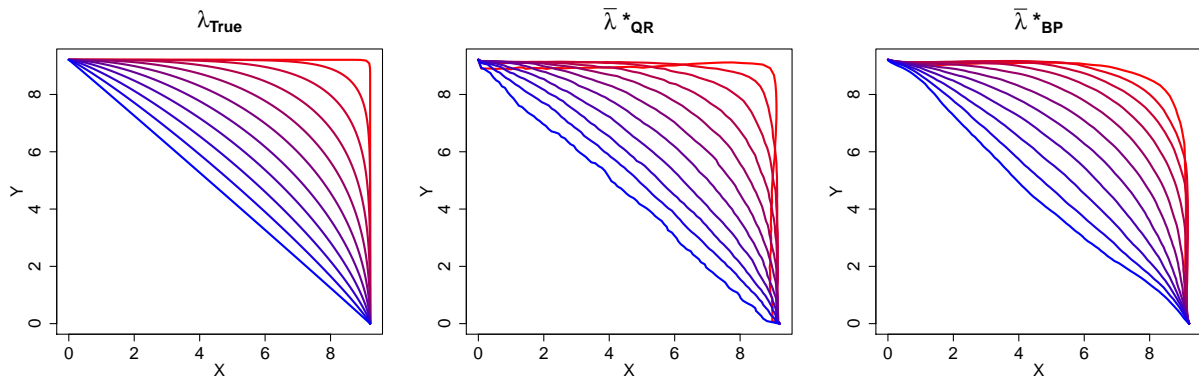


Figure 14: Non-stationary return curve estimates over time for the inverted logistic copula.

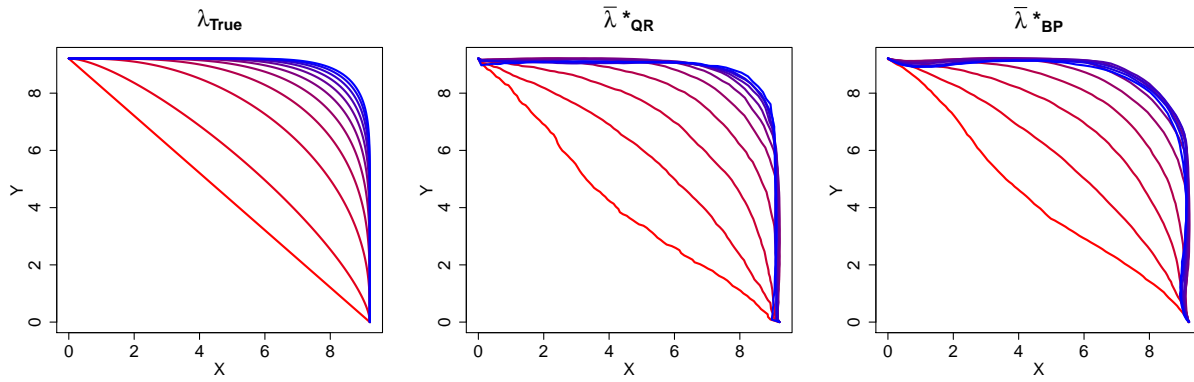


Figure 15: Non-stationary return curve estimates over time for the inverted Hüsler-Reiss copula.

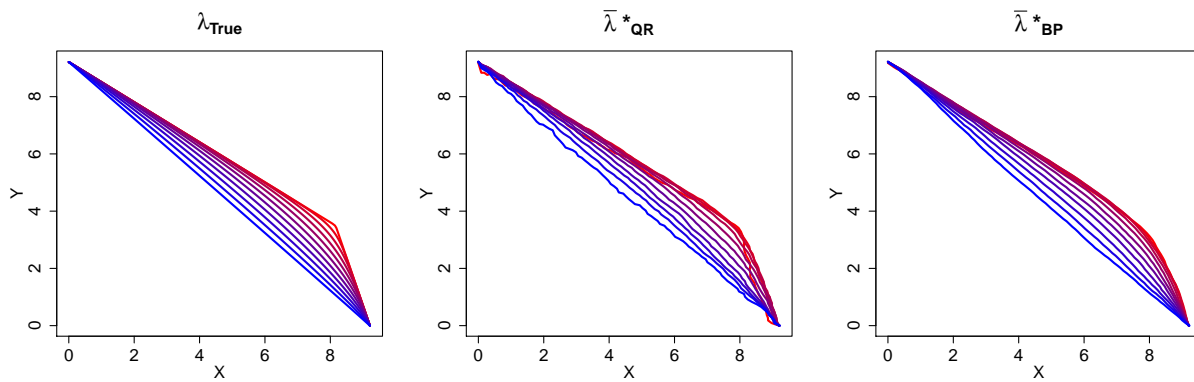


Figure 16: Non-stationary return curve estimates over time for the inverted asymmetric logistic copula.

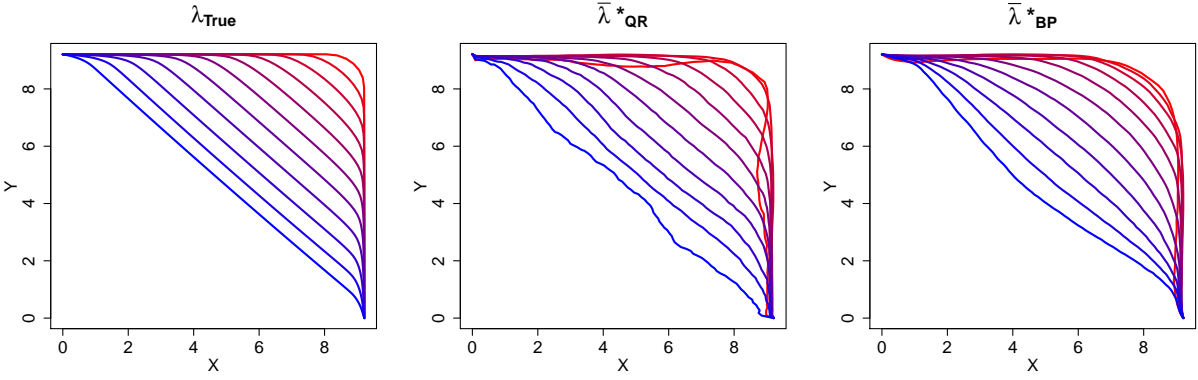


Figure 17: Non-stationary return curve estimates over time for the copula of model (12).

3 Additional case study figures

3.1 Fitted pre-processing trend functions

Figure 18 compares empirical estimates of the mean and standard deviations for both sets of projections against fitted location and scale functions. Empirical estimates are obtained using the data for fixed years over the observation period. The fitted location and scale functions are then averaged over each year and compared to the empirical estimates. One can observe very similar trends for both variables, indicating the pre-processing technique is accurately capturing the marginal non-stationary trends within the body of data.

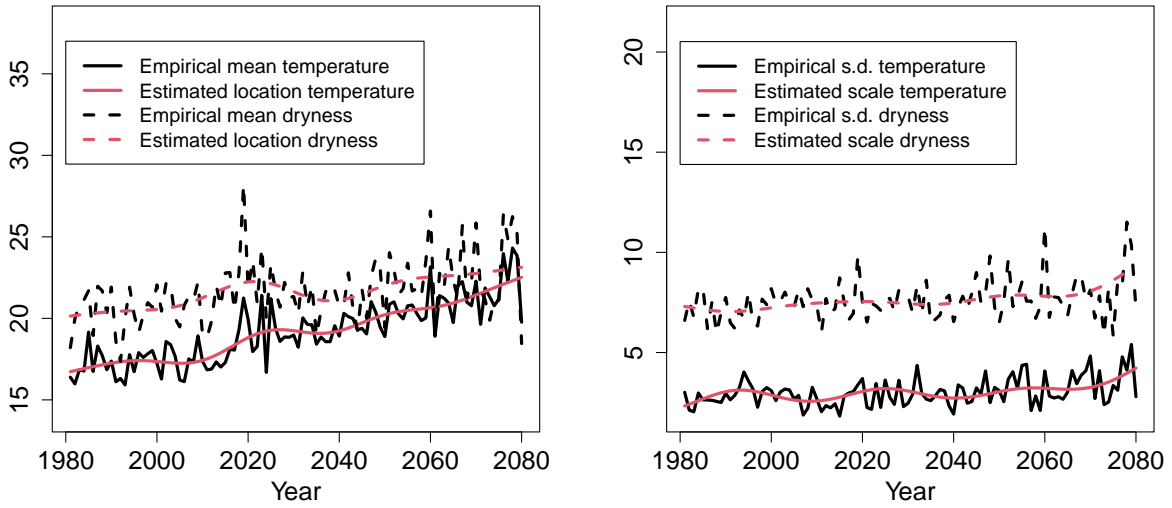


Figure 18: Comparison of estimated location and scale function values (red) against empirical mean and standard deviation estimates (black). For the fitted functions, the average value for a given year has been taken to ensure correspondence with the empirical values.

3.2 Estimated rate parameters

Figure 19 illustrates exponential rate parameter estimates for the pre-processed data, alongside 95% pointwise confidence intervals, for ± 15 year rolling windows over the observation period. As can be observed, the rate parameter estimates remain approximately constant at one throughout the entire observation period, suggesting a successful transformation to exponential margins.

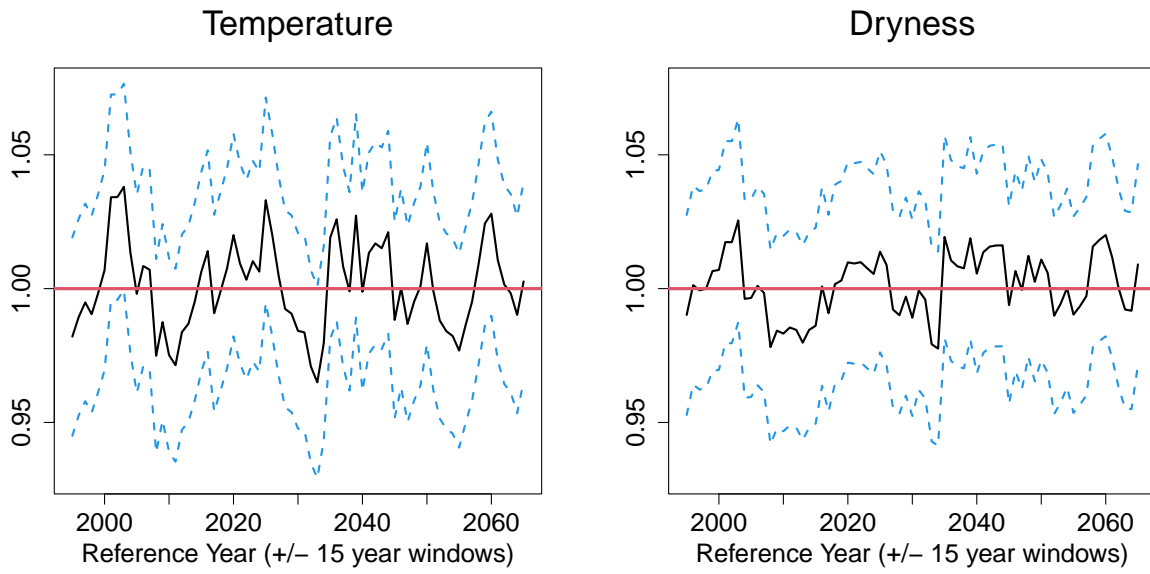


Figure 19: Estimated exponential rate parameters (black) with 95% pointwise confidence intervals (dotted blue) over the time period. The target rate parameter is given in red.